Comparative analysis of Rayleigh and Love waves detected propagating in the Nobi and Kanto basins during the 2004-, 2007- Chuetsu and 2011 Tohoku earthquakes

Kristel Meza-Fajardo, Hideo Aochi, Apostolos Papageorgiou

Comparative analysis of Rayleigh and Love waves detected propagating in the Nobi and Kanto Basins during the 2004-, 2007- Chuetsu and 2011 Tohoku earthquakes

By

Kristel C. MEZA FAJARDO(*) , Hideo AOCHI and Apostolos S. PAPAGEORGIOU

Submitted to

Soil Dynamics and Earthquake Engineering

(*) Corresponding author

ABSTRACT

Propagation of long-period ground motion in sedimentary basins has been a subject of great interest among seismologists and engineers. Intense long-period ground motions consist primarily of surface waves that get trapped or generated locally as seismic energy travels through sedimentary deposits. In the present work, we investigate the propagation of surface waves in the basins of Kanto and Nobi in Japan, during three relatively recent events: The Mw 6.6 2004 Niigata Chuetsu, the Mw 6.6 2007 Chuetsu-Oki and the Mw 9.0 2011 Tohoku earthquakes. We identify the surface waves using a signal processing technique that detects their polarization characteristics, in the time-frequency space, using orthogonality relations among phase vectors. Then, by applying the "Normalized Inner Product" (NIP), regions of a particular type of polarization are delineated and filters are applied to isolate the associated surface waves, along with their direction of propagation. With our investigation, we attempt to follow the '*flow*' of seismic energy as it approaches just outside the basins, and then how it evolves once inside the basin. Our analysis shows that the long period (< 0.1 Hz) surface wave energy approaching the Kanto basin during the 2011 Tohoku earthquake consists of Rayleigh waves, and that part of the seismic energy is converted to Love waves. In a higher frequency range (0.1 – 0.5 Hz), prograde Rayleigh and Love waves were detected in selected areas such as the Chiba sub-basin and the Tokyo lowlands. Regarding the Nobi basin, we find that whereas the Rayleigh waves in the frequency range (0.1 – 0.5 Hz) radiated during the 2011 Tohoku earthquake strongly interact with the basin, the Rayleigh waves radiated by the Chuetsu events appear to propagate through the basin unaffected. This difference in basin response is attributed to the different azimuthal direction of incidence of the surface wave energy.

Keywords: surface waves, Rayleigh, Love, retrograde, prograde, polarization, wave identification

Introduction

The influence of sedimentary deposits in the form of basins on the intensity of strong ground motion has been recognized by Gutenberg [1] since the middle of the previous century. Starting with the seminal theoretical works of Aki and Larner [2] and Bard and Bouchon [3], [4], and the observational study by King and Tucker [5], great progress has been made in addressing the response of sedimentary valleys to incident seismic waves and the body of published literature on the topic is voluminous. Key earthquake events have provided ample evidence of basin-induced surface waves; among them: the 1967 M_w6.6 Caracas earthquake [6], the 1985 M8.1 Michoacan earthquake [7], the 1989 M_S7.1 Loma Prieta earthquake [8], the 1995 M_W 6.9 Kobe earthquake [9], the 2001 M6.8 Nisqually earthquake [10], and the 2003 M_W8.0, Tokachi-Oki earthquake [11], [12]. The earthquake engineering community is also well aware of basin effects, as recent earthquake events (including the megathrust Mw 9.0 2011 Tohoku earthquake) have exposed the effects of long-period ground motions on large-scale structures, such as high-rise buildings, long-span bridges, fluid-filled tanks, etc. (e.g. [11], [13]).

Many studies in Japan focusing on the Kanto and Osaka basin [14]–[20] have observed late-arriving surface waves which have been attributed to a generation process at the edges of the respective sedimentary basins. For basins like Los Angeles basin in California, researchers like Olsen [21], have reported that intense long-period (0 – 0.5 Hz) ground motions can be generated by events located far from the basin edge. Other studies have focused on the effect of the azimuthal angle of long-period seismic waves in basins in Japan [22]–[25]. Surface waves have been also identified via array analysis, in the long period range in microseismic events (*e.g.*, Seydoux *et al.* [26]), and in the intermediate period range in noise measurements (*e.g.*, Wathelet *et al.* [27]). While most of the published literature recognizes the role of surface waves on the

amplification of long period ground motion in sedimentary basins, precise analyses of the propagation of surface waves are difficult to find, in particular analyses from strong ground motion recordings. A few distinctive studies of this kind, early on, are the wave propagation analyses of ground motion recordings in three sedimentary valleys in Central Asia [28], in the Los Angeles basin [29], [30] and in the Mexico Valley [31]. Part of the problem is the fact that surface waves are present in a seismogram along with other types of waves with similar frequencies and arrival times, and their separation has not been a straightforward task. Furthermore, most basins had not been instrumented with seismic networks dense enough as to allow the mapping of the propagation of the different phases. In the last three decades, the nationwide seismic networks (KiK-net, K-NET) in Japan have recorded major, strong events that have generated intense surface waves. These networks have been deployed with a relatively high density, and with instruments capable to record broad-band strong ground motion with high precision.

In the present work, we study surface wave propagation from strong ground motion recordings, by exploiting the dense seismological K-NET network, in both the Nobi and Kanto basins. The Nobi basin in Japan is a sediment filled valley extending over an area of about 1800 square kilometers. The city of Nagoya, being the fourth-most-populous urban area in Japan with more than 2 million people, is located on the basin. The city has suffered extensive damage during large earthquakes in the past, the 1891 M ~ 8 Nobi earthquake being the most dramatic example [32]. Similarly, the Kanto basin, where Tokyo, the capital of Japan, is located, sustained heavy destruction during the 1923 M ~ 8 Kanto earthquake (e.g. [33]).

We analyze the strong ground motion recordings using a recently proposed method (referred to as the Normalized Inner Product method – NIP for short) [34] to identify the various

71 types of surface waves and extract them. We study the propagation of the very complex wave-
72 field that was generated by the megathrust 2011 Tohoku earthquake, and two smaller earthquake
73 events, the 2004 Chuetsu and 2007 Chuetsu-oki events. With this investigation, we attempt to
74 track the '*flow*' of seismic energy as it approaches the basin, and inside it. In that effort we try to
75 focus on the composition of the surface wave energy just outside the basin and then inside the
76 basin. We identify the most energetic Rayleigh waves, indicate if they are retrograde or prograde,
77 and provide their direction of propagation. We also identify intense Love waves, extract their
78 waveforms, and estimate their direction of polarization. We establish if the identified seismic
79 energy in the form of surface waves was converted at the basins, or if it arrives to the basins
80 already in the form of surface waves. Our study, among other things, demonstrates the power of
81 the NIP method in analyzing complex wave-fields.

82 This work is organized in terms of the three earthquake events under study. We first
83 describe the structure of the two basins and briefly present the method of identification of surface
84 waves. Next we compare the surface wave fields generated by the events mentioned above,
85 focusing on the different basin responses. The first event that we present is the Tohoku
86 earthquake, a major event which, due to its large faulting area, radiated to the two basins from a
87 range of azimuthal directions. We then present the Chuetsu and Chuetsu-oki earthquakes
88 together, as these two events have very similar magnitude and similar mechanism and their
89 epicenters are very close to each other.

90 **Sedimentary basins**

91 The Nobi basin, located in the central part of Japan (Figure 1a), is a basin with a
92 maximum depth of 3 km composed of Alluvial, Pleistocene and Tertiary strata [35]. On the other
93 hand, the well-known Kanto basin is a deep and geometrically more complex sedimentary basin

94 with an inland bedrock depth as large as 4 km under the Chiba prefecture [36]. The Kanto basin
95 is composed of Quaternary and Tertiary sediments, surrounded on the north and west by
96 mountains composed of volcanic and Pre-Tertiary rocks [16]. Figures 1 and 2 show the bedrock
97 depth of the two basins, indicated by the depth of the layer corresponding to Vs=2700 m/s,
98 retrieved from the 3D national deep structure model of the National Research Institute for Earth
99 Science and Disaster Resilience of Japan [37]. According to Figure 2, the Nobi basin can be
100 considered as one concave deposit of soft layers whereas the geometry of the Kanto basin
101 includes deposits in the form of several elongated branches. As the maximum depths of the Nobi
102 and Kanto basins differ significantly when compared to each other, we can expect different basin
103 responses to the incoming wave fields. We also note in Figure 2 that, for both Kanto and Nobi,
104 the basin edges are steeper on their western sides.

105 **Earthquake events and recording stations**

106 The source parameters of the three events considered in this study are listed in Table 1,
107 where we note that the Chuetsu and the Chuetsu-oki earthquakes have the same magnitude and
108 similar focal depth. In addition of being closely located, the focal mechanisms for these two
109 earthquakes can be considered virtually identical. Several studies (Furumura and Hayakawa [13],
110 Yoshimoto and Takemura [34]) have already reported the observation of important long period
111 motions associated to these earthquakes. Differing from the Chuetsu and Chuetsu-oki
112 earthquakes by its great size and its location at a subduction zone, the wave field radiated by the
113 Tohoku earthquake allows the observation of different aspects of basin response.

114 In this study we analyze accelerograms of flat broadband response recorded by the K-
115 NET seismographic network [39] at rock outcrop sites and sites within the basins. The spatial
116 distribution of the stations considered in the study is shown in Figures 1b and 1c, although not all

stations recorded all three events. We identify and extract Love ad Rayleigh waves based on their characteristic elliptical polarization, which requires that we work with displacement histories. These displacement histories were derived from the recorded acceleration histories, by band-pass filtering between 0.05 and 20 Hz with a second order Butterworth filter, and then integrating in time twice. Figure 3 shows the three components of displacement waveforms at two stations on rock, station GIF024 in Nobi, and station SIT006 in Kanto, during the three events listed in Table 1. We can observe that the frequency content and duration seem very similar during the two Chuetsu events. Furthermore, the displacement amplitudes recorded at the two stations, are comparable (if not the same) for the two events. On the other hand, the amplitudes of the Tohoku earthquake recordings are an order of magnitude greater, as compared to those of the Chuetsu events, clearly because of its great size.

Identification and extraction of surface waves

To study the propagation of surface waves, we make use of a signal processing technique [34] that allows the identification and extraction of wave packets of Rayleigh and Love waves, along with their direction of maximum energy. In the context of waves trapped in a basin, wave packets of different frequencies can simultaneously arrive at a station of interest, and thus the analysis benefits from resolving the signal in the time-frequency domain, by means of the Stockwell Transform [40]:

$$S(t,f) = \int_{-\infty}^{\infty} h(\tau) \frac{|f|}{\sqrt{2\pi}} \exp\left[-\frac{(t-\tau)^2 f^2}{2}\right] \exp(-2\pi i f \tau) d\tau \quad (1)$$

where $h(t)$ is the time-function that is being transformed. Each component of the recorded motion becomes a complex-valued matrix defined in the discrete time-frequency (t, f) space. Equivalently, each complex-valued entry of the matrix may be described by a *phasor* (or *phase*

138 *vector*, i.e. a vector defined by the magnitude and the phase/argument of the complex number that
139 it describes; [41]). In Figure 4 we show the amplitudes of the S-transform (i.e. the magnitudes of
140 the phasors) of the vertical components of displacement waveforms presented in Figure 3. We
141 can readily observe in Figure 4 that the dominant frequencies for the two Chuetsu events are in
142 the frequency range 0.1-0.2 Hz, whereas for the large Tohoku earthquake the dominant frequency
143 is below 0.1 Hz. These observations remain consistent for the two stations that are far from each
144 other, one near the Nobi basin and the other near the Kanto basin. Because stations GIF024 and
145 SIT006 are considered to be located on rock, we attribute the observed dominant frequencies to
146 the source characteristics and, possibly, to the propagation path. In particular, the low frequencies
147 (less than 0.1 Hz) observed in the recordings of the Tohoku event, are attributed to the large
148 dimensions of the rupture (e.g. [42]–[44]). However, Figure 4 also shows that the energy radiated
149 by the Tohoku earthquake in the frequency range 0.1-0.5 Hz is still important, and in the sequel,
150 we investigate its interaction with the basins.

151 The basic idea of the method to extract Rayleigh waves, presented by Meza-Fajardo *et al.*
152 in [34], is to identify regions in the time-frequency space where the particle polarization is
153 elliptical. Because ellipticity is a parameter which rapidly changes in a seismogram, we prefer to
154 identify elliptical polarization by the orthogonality of appropriate phasors of the transformed
155 wave train. We look for regions in the (t, f) space where there is a $\pm(\pi/2)$ phase shift between the
156 phasors of the horizontal and vertical displacement components. This reasoning then leads
157 naturally to the use of the inner product as a tool to identify orthogonality between phasors. The
158 inner product will be zero if the phasors are orthogonal. Furthermore, if the phasors of two
159 components (say the vertical and a horizontal) are orthogonal but one performs a $\pm(\pi/2)$ shift in
160 one of them (say, the phasor of the vertical component of a Rayleigh wave), then the inner

product of the two components will be close to 1, if the phasors are normalized by their magnitudes. As shown in [34], the normalized inner product (NIP) of Rayleigh wave components is a parameter that presents less variation with time and frequency as compared to other measures of ellipticity. Then, we can effectively construct filters in the time-frequency (t, f) space to isolate and retain only those regions where the NIP is close to 1 (say NIP > 0.8), and retrieve the waveforrms (that is, the time histories) of the desired Rayleigh waves by inverting back to the time domain. The extracted Rayleigh waves are retained only if the correlation coefficient between the time histories of the horizontal and (shifted) vertical component is higher than 0.8. On the other hand, the inner product has proved to be useful also in identifying the direction of polarization (or, equivalently of maximum energy) of the horizontal component of a wave train [34], [45], because it can be used to find the two orthogonal horizontal directions for which the correlation is minimum. In the latter case the direction of polarization of Love waves can be also identified. We refer the readers to the previous publications [34], [45] where they can find more details on the wave extraction technique.

In the present work, we implement the filtering technique described above at each station independently, and assuming that the surface wave energy dominating the three-component seismogram corresponds to retrograde Rayleigh waves, as it is the mode most commonly observed in ground motion recordings. Prograde Rayleigh waves are also investigated, especially when the direction of retrograde wave propagation among several stations cannot be verified. Finally, waveforms for Love waves are detected independently at each station after both retrograde and prograde Rayleigh waves have been filtered out of the seismogram.

The 2011 Tohoku earthquake

Surface waves in the lower frequency range (0.05-0.1 Hz)

Figure 5 displays the identified and extracted retrograde Rayleigh waves on both basins in the frequency range 0.05-0.1 Hz. The top panels of Figure 5 illustrate the direction of polarization (this direction is referred to also as the *direction of maximum energy*), and thus, for the case of Rayleigh waves, the direction of propagation, indicated by an arrow at each station where these Rayleigh waves have been identified. The length of each arrow is proportional to the amplitude of the Rayleigh waveform identified at the corresponding station shown in the figure. On the bottom panels, the time histories of selected stations are plotted, showing the two components of Rayleigh waves, the horizontal component in the indicated direction of maximum energy, and the vertical component with a $(\pi/2)$ shift. These two components should be in phase - as they appear to be in the figure - if the extracted waves have elliptical polarization, that is, if indeed they are Rayleigh waves. The intermittent straight line, on the top panels indicates the direction of maximum energy averaged over all stations shown in the figure. The wave-traces shown on the bottom panels correspond to stations that were selected by their close proximity to the intermittent straight line that indicates the average direction of propagation. Furthermore, the separation distances of the wave-traces along the vertical dimension of the bottom panels of Figure 5, are proportional to the separation distances between the projections of the positions of the stations on the intermittent straight line. The waveform plot constructed in this fashion permits us to verify visually the direction of polarization (i.e. direction of maximum energy) of the extracted wave. In the case of Rayleigh waves the direction of polarization coincides with the direction of propagation, and thus the waveform plot should show how the waves propagate in the estimated average direction. For the extracted retrograde Rayleigh waves shown in Figure 5, we can assert that this is, in fact, the case.

For the Rayleigh waves in the Kanto basin of Figure 5a the average direction of propagation has an azimuth of 245 degrees. The consistent direction of propagation from station to station (Figure 5a, top panel) and the very coherent waveforms (Figure 5a, bottom panel) provides convincing evidence of the passage of the long-period (0.05 – 0.1 Hz) Rayleigh wave phase. Deviations from the average direction of propagation may be attributed to lateral variations of the velocity profile of the medium. On the other hand, the Rayleigh waves of Figure 5a in the Kanto basin interact with the northern edge of the basin. Specifically, the incident surface wave energy is diffracted by the edge that is separating the two linear branches of the basin at the north. As a result of this diffraction, part of the incident seismic energy is 'channelled' along the north-western linear branch of the basin. [Parenthetically we note that such 'channeling effects' have been reported by Miyake & Koketsu [46], for basins in Japan, and by Olsen *et al.* [47], for basins in California.] We also identify retrograde Rayleigh waves in the Kanto basin that propagate to the southeast, with an average azimuth of 158 degrees, as shown in Figure 5b. This particular phase is interpreted as being seismic energy diffracted from the steep north-eastern edge of the basin (indicated by the thick solid line in Figure 5b). Figure 5b displays the presence of these waves only at some stations on the southeast quadrant of the basin (around the Chiba area). We also note that there is an amplification of these diffracted waves at the stations located on the deepest part of the Chiba area (for example, stations CHB013 and CHB016).

Figure 6 displays a very different basin response for the extracted retrograde Rayleigh waves propagating in the Nobi basin. The amplitudes of the extracted Rayleigh waves in the Kanto basin are higher (~13 cm) than the amplitudes of the corresponding extracted waves in the Nobi basin (~5 cm); an expected result given that the Nobi basin is farther from the Tohoku

rupturing fault. Furthermore, we note in Figure 6 that as the retrograde Rayleigh waves propagate through the Nobi basin, their amplitude, coherence, and direction of propagation is only slightly affected. In contrast to the diffraction phenomena observed in the Kanto basin, we find that because of their long wavelength (relative to the basin depth), the identified Rayleigh waves do not interact with the Nobi basin.

Focusing in the Chiba area and working always in the lower frequency band (0.05 – 0.1 Hz), we find in the recorded motions the presence of *Love waves* of significant amplitude, as shown in Figure 7. The arrows without head on the left panel of Figure 7 indicate the direction of linear polarization of the extracted waves. Keeping in mind that the direction of propagation of the Love waves is expected to be normal to their direction of linear polarization, we estimate an average direction of propagation of 215 degrees, not very different from the direction of propagation of the Rayleigh waves of Figure 5a (on the western part of the Chiba area). However, the direction is quite different from the direction of propagation of the Rayleigh waves of Figure 5b observed on the eastern part of the Chiba area. These results indicate that 0.05-0.1 Hz Rayleigh waves arriving to the Kanto basin are not only being diffracted at its northern edge, but also they are being converted to Love waves in the Chiba area. We also note that the identified Love waves are detected mainly in the deepest parts of the basin, having significantly reduced amplitudes when they reach the Chiba sub-basin edges. Along with the diffracted Rayleigh waves identified earlier for the Chiba area (Figure 5b), we can consider them as *basin-generated* surface waves.

Surface waves in the higher frequency range (0.1-0.5 Hz)

Figure 8 and 9 display the Rayleigh waves identified in the range 0.1-0.5 Hz propagating through the Kanto and the Nobi basin, respectively. The figures were composed following the same

252 procedure used in Figure 5. The identified waves are not as strong as the corresponding waves in
253 the range of 0.05-0.1 Hz, but being associated with higher frequencies and having amplitudes
254 beyond 6 cm they can potentially have a detrimental effect on engineering structures (e.g., Meza-
255 Fajardo and Papageorgiou [48]). For this higher frequency range, it is clear from Figure 8 and
256 Figure 9 that the incident seismic wave-field interacts strongly with the two basins, as the
257 direction of propagating of the extracted waves varies significantly among stations, and the
258 coherency is rapidly lost as the waves propagate. Furthermore, in the case of the Kanto basin we
259 identify both retrograde and *prograde* Rayleigh waves, shown in Figures 8a and 8b respectively.
260 This finding is illustrated in Figure 10, where we plot the particle motion in the vertical plane
261 oriented in the direction of propagation at stations SIT001 and CHB006. Figure 10a clearly
262 shows that the first Rayleigh wave train identified at station SIT001 (between 120-140 s) is
263 retrograde, as the sense of rotation is opposite to the direction of propagation (given by the
264 positive sense of R; R denotes direction of maximum energy or direction of propagation). For
265 station CHB006 (Figure 10b) we selected the second wave train (between 130-150 s) because its
266 low frequency allows for a clearer drawing of the ellipse, and a prograde particle motion is
267 indeed observed.

268 In Figure 8a we observe multiple wave trains of retrograde Rayleigh waves at most selected
269 stations. These wave trains are responsible for the long duration of the motion in the basin. By
270 looking at the size of the arrows, which is proportional to the amplitude of the extracted waves,
271 we observe that the strongest waves are identified in the deepest parts of the Chiba and Gunma-
272 Saitama areas. As expected, the identified Rayleigh waves arrive with strong intensity from the
273 east, and as they leave the basin on the western edge, they are significantly less energetic, due to
274 the strong interaction with the Kanto basin. In the case of the prograde waves (Figure 8b), the

strongest wavetrains are found in the Chiba and the Tokyo bay area. When compared to the retrograde Rayleigh waves, we note that these prograde waves arrive at the stations at relatively later times, which suggests that they are a very localized basin effect. This observation is reinforced by the fact that in Figure 8b prograde waves are identified only within the basin and only in its eastern part. Then, it is reasonable to conclude that the prograde waves, identified both in the Tokyo bay area and in the Chiba area, are *basin-generated* Rayleigh waves and they are in the frequency range of 0.15-0.2 Hz (that is, 5-6.7 s). These results are consistent with those of Boué *et al*. [49], who had already pointed out a prograde mode between 4.7 and 7.6 s for the Kanto basin from analyses of ambient seismic fields. In passing we mention that Tanimoto and Rivera [50], on the basis of theoretical analysis, attribute prograde Rayleigh wave particle motion to the existence of very slow (i.e. soft) deposits on top of very thick sediments.

A different response is observed with the retrograde Rayleigh waves identified in the Nobi basin, shown in Figure 9. A coherent pulse with central frequency of 0.15 Hz is identified at the borders of the basin at stations GIF024 and AIC009, but as the energy reaches the deeper parts of the basin, the pulse is no longer distinguishable. On the other hand, we observe an elongated duration of the Rayleigh waves at station AIC011 which is located in a deeper part of the basin. The longer duration is a consequence of seismic energy being trapped in the basin. This energy, in the form of surface waves, traverses the basin more than once, after being reflected at the edges of the basin. An interesting observation regarding Figure 9 is that although the overall direction of propagation in this higher frequency range (0.1 – 0.5 Hz) is westward, the seismic energy, when it reaches the western, steeper edge of the basin, is partially reflected, while most of the seismic energy is diffracted to the south (this is clearly evident in the record MIE009). The latter phenomenon is reminiscent of a similar diffraction of the incident seismic energy caused by

298 the Hachioji line at the western edge of the Kanto basin, reported for Love waves by Kinoshita et
299 al. [15], and Koketsu and Kikuchi [49].

300 In Figure 11 we present the extracted Love waves in the Kanto basin in the range 0.1-0.5 Hz.
301 The intermittent line in the map indicates an estimate of the direction of propagation of the Love
302 waves considering it should be normal to the direction of polarization. We observe in Figure 9
303 that the direction of propagation of the Love waves is to the south-west, clearly different from the
304 direction of propagation of the Rayleigh waves in the same frequency range (Figures 8a and 8b).
305 However, the direction of propagation of these Love waves (Figure 11) remains very close to the
306 direction of propagation of the lower frequency (0.05-0.1 Hz) Love waves of Figure 7. We also
307 note that for both frequency ranges, most Love waves are polarized in a direction *parallel to the*
308 *northern edge of the Kanto basin*. The amplitudes of these waves are remarkably higher as they
309 are more than two times the amplitude of the Rayleigh waves identified in the same frequency
310 range. With an amplitude of 15 cm and with a central frequency of 0.14 Hz these waves can
311 subject high-rise buildings and long-period structures to potentially destructive torsional
312 excitation (e.g., Cao *et al*. [52]). Furthermore, Figure 11 clearly shows that the southern part of
313 the Kanagawa area is not much affected by these Love waves, and it is the Tokyo bay and
314 northwestern Chiba areas where they are much stronger. The amplitudes of these Love waves
315 appear significantly reduced in the southern stations of the Chiba area, and they are negligible
316 outside the basin, suggesting that these waves too are *basin-generated* surface waves.

317

Quantitative characterization of surface waves in the Kanto basin

In this section we proceed to quantify basin effects by analyzing the surface waves previously identified, focusing on the waves that we have characterized as 'basin-generated'. We consider only the basin-generated waves in the frequency range (0.1-0.5 Hz), since basin effects at lower frequencies are not relevant for engineering structures. We quantify the surface waves under investigation using two parameters: (1) central frequency f_o, which is defined as the frequency associated with the maximum amplitude of the S-Transform of the extracted waves; and (2) amplification coefficient A.

Typically, the definition of amplification necessitates the use of a reference station on rock. However, in the present case, this is not possible as 'basin-generated' waves exist only in the sediments of the basin and do not exist on rock. We proceed to estimate amplification of the prograde Rayleigh and the Love waves extracted at the Kanto basin in the frequency range (0.1-0.5 Hz) by considering two different definitions of the coefficient of amplification A. One way to quantify amplification is by using the amplification coefficient A_1 defined as follows:

$$A_1 = \frac{\max_t |S_O(t,(f_o)_O)| \cdot (f_o)_R}{\max_t |S_R(t,(f_o)_R)| \cdot (f_o)_O} \tag{2}$$

where $S_O(t,f)$ is the Stockwell Transform of the extracted waves at a station of 'observation', and $S_R(t,f)$ is the Stockwell Transform of the extracted waves at a 'reference' station. By necessity, both stations are located inside the basin. Frequencies $(f_o)_O$ and $(f_o)_R$ are the central frequencies of the extracted waves at the station of 'observation' and the 'reference' station, respectively. The ratio of Eq. (2) then takes into account the fact that we are comparing wave amplitudes of different frequencies, a necessary consideration when analyzing dispersive wave packets [53]. Furthermore, to minimize interference with other type of surface waves (Love

339 waves for example), we use the vertical component to measure the amplification coefficient of
340 the Rayleigh waves. As 'reference station', we select a station that is at the beginning of the
341 wave-path of the basin-generated waves, where these particular waves are at their inception. In
342 Figure 12a we show the spatial distribution of the central frequency of the identified prograde
343 Rayleigh waves, and in Figure 12b the corresponding amplification coefficient A_1. Based on
344 Figure 8b, we selected station CHB005 as the reference station. For a better illustration of the
345 results, in Figure 12a we size the circles according to the amplification coefficient shown in
346 Figure 12b. Figure 12 illustrates not only that the prograde Rayleigh waves are stronger at the
347 northern edge and on the Chiba sub-basin, but also the dominant frequency associated with these
348 waves decreases as they reach the southern edge of the basin. Evidently, depth of the sediments
349 appears to be the controlling factor of the central frequency of these waves.

350 Figure 13 displays the central frequency and amplification coefficient of the extracted Love
351 waves. Based on Figure 11, we selected station IBR012 as the reference station, at which the
352 extracted waves have a central frequency of 0.46 Hz. To estimate the amplification coefficient for
353 Love waves we use the horizontal component in the direction of polarization (direction of
354 maximum energy) shown in Figure 11. First, we observe that the central frequency of the Love
355 waves is in most stations lower than that of the prograde Rayleigh waves. Figure 13 also displays
356 that the spatial distributions of the amplification coefficients, associated with Love and prograde
357 Rayleigh waves, differ significantly. The strongest amplification of Love waves is concentrated
358 more in the Tokyo bay area and along the northern part of the Chiba sub-basin. Let us note that
359 the generation of Love waves during the Tohoku earthquake in this frequency range was
360 remarkable, having reached values of amplification coefficient A_1 as high as 35.

However, amplification as defined by coefficient A_1 (Eq. 2), is associated with two weaknesses: (1) Selection of the reference station is subjective and, depending on the distribution of stations, may not always be feasible; (2) being associated with the ratio of spectral amplitudes at two specific frequencies, the value of the ratio is expected to be very sensitive and, accordingly, it may vary significantly over a wide range. Stating this differently, one would need a very large number of recordings to obtain statistically significant, and therefore useful, average estimates of amplification. To circumvent both difficulties, we propose an alternative definition for the coefficient of amplification; we refer to this alternative definition of amplification coefficient as A_2. Specifically, based on the definition of the Stockwell transform, it is evident that $|S(t,f)|^2$ is proportional to an estimate $\hat{G}_{xx}(t,\omega)$ of the (one-sided) evolutionary Power Spectral Density (PSD) function of the stochastic process, a realization of which is the signal (strong motion recording) under analysis [54], [55]. Specifically, $\hat{G}_{xx}(t,2\pi f) = \left(2\sqrt{\pi}/f\right)|S(t,f)|^2$. We proceed to define a '*frequency function*' $\mathbb{S}_E(f)$ (which is a measure of the energy of the signal at frequency f) and its average value $\mathbb{S}_E^{av}$ for the range of frequencies $f_\ell < f < f_\hbar$ over which the energy of the signal is distributed :

$$\mathbb{S}_E(f) = \int_0^\infty \frac{|S(t,f)|^2}{f}\, dt \qquad \mathbb{S}_E^{av} = \frac{1}{(f_\hbar - f_\ell)} \int_{f_\ell}^{f_\hbar} \mathbb{S}_E(f)\, df \tag{3}$$

The frequencies f_ℓ and $f_\hbar$ are selected so that $\int_0^{f_\ell} \mathbb{S}_E(f)\, df / \int_0^{+\infty} \mathbb{S}_E(f)\, df = 0.005$ and $\int_0^{f_\hbar} \mathbb{S}_E(f)\, df / \int_0^{+\infty} \mathbb{S}_E(f)\, df = 0.995$. This approach is adopted to avoid frequency ranges at the margins, over which the energy is practically zero, which biases the value of $\mathbb{S}_E^{av}$. Based on the above considerations, we define the alternative amplification coefficient A_2 as follows :

$$A_2 = \sqrt{\frac{\mathbb{S}^{av}_{E\_TOTAL}}{\mathbb{S}^{av}_{E\_BODY}}} \quad (4)$$

where $\mathbb{S}^{av}_{E\_TOTAL}$ is associated with the *total* signal (i.e. all phases / types of waves are included), while $\mathbb{S}^{av}_{E\_BODY}$ is associated with the signal after surface waves have been extracted and only body waves remain in the signal. It should be pointed out that A_2 appears to be a stable measure of amplification, unlike A_1 which is sensitive to the choice of a reference station and to the specific frequencies involved in its definition. Evidently, if there are no extracted surface waves in the strong motion record, then $A_2 = 1$. It must be pointed out that A_2 measures the amplification of surface waves relative to the body waves of the same station which themselves may undergo a measure of amplification due to the presence of the sediments.

Figures 12a and 13a display the central frequency f_o and the amplification coefficient A_1 of prograde Rayleigh and Love waves, respectively. The central frequency f_o appears to be controlled by the depth of the sediments for both types of surface waves (Figures 12a and 13a). Regarding the amplification coefficient A_1, the picture appears to be rather clear for Love waves (Figure 13b): A_1 appears to increase with the depth of the sediments, as one moves away from the northern edge of the Chiba sub-basin which apparently was the diffractor that generated these waves. Turning our attention to the amplification of the prograde Rayleigh waves, as measured by the coefficient A_1 (Figure 12b), the results indicate that the highest amplifications are registered in the vicinity of the deepest parts of the Chiba sub-basin.

Considering now the amplification coefficient A_2, shown in Figures 14b and 14d, we observe that the values A_2 obtained are much lower than the corresponding coefficients A_1. Let us recall that A_2 has a different meaning than A_1, since it measures how much the surface waves increase the body wave energy in a frequency range at a station. Therefore, it is not surprising that the two

401 coefficients A_1 and A_2 give different results, and the choice between the two should be based on
402 the analyst's objectives. However, we note that for both coefficients A_1 and A_2, the amplification
403 of Love waves is consistently higher as compared to amplification of Rayleigh waves.
404 Furthermore, for both A_1 and A_2, the amplification of Love waves (Figure 14d) is strong in the
405 neighborhood of the northern edge of the Chiba sub-basin while it is lower everywhere in the
406 southern part of the area. On the other hand, for prograde Rayleigh waves the values of A_2 do not
407 exceed 1.5 and the highest values are in the area of the northern edge of the Chiba sub-basin
408 (Figure 14b). The spatial distributions of the amplification coefficients A_1 and A_2 are very
409 different, since the highest values of A_1 are located in the deepest part of the Chiba sub-basin
410 (Figure 12b), mainly in part due to the very low central frequencies identified in that region.

411 Another parameter that may be computed from energy estimations via de S-transform is the
412 relative group delay time t_{dr}, which is defined as the time delay of arrival of the maximum
413 amplitude of the S-Transform of the extracted wave relative to the time of arrival of a reference
414 frequency f_r:

$$t_{dr} = \frac{\int_0^\infty t \cdot |S_{SW}(t, f_o)|^2 dt}{\int_0^\infty |S_{SW}(t, f_o)|^2 dt} - \frac{\int_0^\infty t \cdot |S_{BODY}(t, f_r)|^2 dt}{\int_0^\infty |S_{BODY}(t, f_r)|^2 dt} \quad (5)$$

415 Since in the recordings we observe basin effects at frequencies below 1 Hz, we select 2 Hz as
416 the reference frequency f_r. We associate this reference frequency f_r to body waves, regarding
417 possible dispersion effects for these waves as not significant. On the other hand, surface waves
418 are known for propagating as highly dispersive wave packets and usually having a late arrival
419 time, elongating the duration of the signal, and thus the relative time delay is a parameter of
420 interest to quantify surface waves. Eq. (5) (above) makes feasible the automation of the process
421 of t_{dr} determination. Figures 14a and 14c display the relative group delay time t_{dr} of the

prograde Rayleigh and Love waves, respectively, in the 0.1-0.5 Hz frequency range. We observe that the relative time delay of Love waves is more organized in space compared to that of the prograde Rayleigh waves. For both prograde Rayleigh and Love waves, we observe that the maximum values of t_{dr} are similar and that they are located in the Tokyo lowlands, finding also high values of t_{dr} at the Chiba sub-basin. Those are the regions where the identified surface waves (especially Love waves) have very low central frequencies, suggesting that the dispersion of surface waves is highly influenced by the local geological structure.

The Chuetsu and Chuetsu-oki earthquakes

Surface waves in the frequency range (0.1-0.5 Hz)

We perform a similar surface wave analysis for the Chuetsu and Chuetsu-oki events, but now we focus only in the frequency range 0.1-0.5 Hz, as this is the frequency range we identified in Figure 4 for these two events. Also, due to space limitations we only estimate the central frequency of the extracted waves and the amplification coefficient A_1. In Figures 15 and 16 we present the waveforms and direction of propagation of the retrograde Rayleigh waves identified on the recordings of the basins. We start again with the Nobi basin (Figures 15a and 15b), which is receiving seismic radiation by these two events from the northeast. Retrograde waves with the same central frequency (0.13-0.15 Hz) arrive to the Nobi basin during both Chuetsu earthquakes, the Rayleigh waves from the Chuetsu-oki event being more energetic. From Figure 15 we make the following observations: (i) there is little loss of coherency among stations located at very different points on the Nobi basin, (ii) the direction of propagation of the extracted waves is similar among stations, and (iii) amplification is present only at stations MIE003, located over the deepest part of the basin. The extracted Rayleigh waves identified previously (Figure 9) for the

445 Tohoku earthquake have similar central frequency, but apparently the incident seismic field has a
446 broader frequency content, as compared to the almost monochromatic incident wave-field of the
447 two Chuetsu events (Figures 15a, b). Furthermore, the Nobi basin receives radiation from both
448 Chuetsu events over a very narrow range of azimuthal angle (practically from one azimuthal
449 angle) while in the case of the Tohoku event the basin receives radiation over a wider range of
450 azimuthal angles, due to the very large size of the Tohoku source.

451 In the Kanto basin we observe that the propagation of retrograde Rayleigh waves is again
452 similar for the two Chuetsu earthquakes (Figures 16a and 16b). A Rayleigh wave train of shorter
453 duration (relative to that of Nobi), propagates with an average azimuthal direction close to 120
454 degrees, and is amplified at stations GNM008 and GNM010. We observe same amplitudes and
455 frequencies at several stations that recorded the two events, for example, stations GNM010 and
456 CHB005. After leaving the narrow channel-type structure the wave train is reduced in coherency
457 and amplitude, as it is scattered and 'diffused' within the basin. A coherent wave train can be
458 identified (for both events) traveling south along the edge of the basin, osculating the western
459 edge of the basin and, interestingly, no retrograde Rayleigh waves are detected in the deepest
460 parts of the Kanto basin. The phases observed on stations IBR014 and CHB005 for the Chuetsu
461 earthquake, and on stations CHB004 and CHB005 for the Chuetsu-oki earthquake, may be
462 dispersed (and possibly diffracted) versions of the corresponding phases observed earlier in the
463 narrow channel-type structure.

464 In Figures 17(a) and (b) we present the prograde Rayleigh waves identified at the Kanto
465 basin during the two Chuetsu events. Considering the randomness inherent to all seismic events,
466 there is a striking similarity among the waveforms and the spatial distribution of the stations
467 where prograde waves were identified during the two events. The waveforms identified on the

468 recordings of stations located in the Tokyo bay area have strong amplitudes [as indicated by the
469 arrows in Figures 17(a) and (b)], and they also have a significantly longer duration, relative to the
470 retrograde waves. Let us note that numerous long-period high-rise buildings are located in the
471 Tokyo bay area, which can be significantly affected by these waves having central frequencies in
472 the range 0.12-0.16 Hz. During the Tohoku earthquake the prograde waves in the Tokyo bay area
473 propagate along an East-West direction (see Figure 8b), whereas for the Chuetsu events they
474 propagate along an average azimuthal direction close to 150 degrees, which suggests that these
475 prograde waves propagate in the Tokyo bay area without a preferred direction related to the basin
476 structure. Finally, the maps in Figures 17(a) and (b) show how these prograde waves become
477 weaker and diffracted as they approach the southeastern border of the basin.

478 Next, we turn our attention to the Love waves identified in the Kanto basin during the
479 Chuetsu events, the time histories of which are displayed in Figures 18(a) and (b). We observe
480 that the most energetic Love waves are present in the Saitama-Tokyo area, including the Tokyo
481 bay area. In the Chiba area the amplitude of the Love waves is considerably smaller, even though
482 the basin reaches its maximum depth in this area, illustrating once more the importance of the
483 azimuthal direction of the energy arriving at the basin. It is worth pointing out that once again the
484 Love waves identified near the northern edge of the basin are polarized in a direction parallel to
485 that edge. The waves identified close to the western edge (which is oriented along a north-south
486 direction) of the Kanto basin are also polarized in a direction parallel to the edge. That Love
487 waves can be generated by the north-western edge of the Kanto basin has been suggested by
488 Kinoshita et al. [15], based on observations from previous events arriving from the southwest.
489 Furthermore, this 'behavior' of Love waves polarized parallel to the edge of a basin has been
490 already observed in other basins, like Los Angeles basin [56].

491 *Amplification of surface waves in the Kanto basin*

492 In the previous section, we illustrated how the two (very similar) Chuetsu events
493 reproduced very closely the propagation of the simple Rayleigh retrograde wave-train arriving to
494 the Kanto Basin from the northwest, along with the generation of Love and prograde Rayleigh
495 waves. The similarity is more evident when we map the central frequencies and amplification
496 factors of the extracted waves. In Figures 19 and 20 we present the quantification of these
497 parameters for the waves that we consider 'basin-generated' (the prograde Rayleigh and Love
498 waves). Stations GNM010 and GNM013 were selected as reference stations for Love and
499 prograde Rayleigh waves, respectively. Note that even though station GNM009 is at the
500 beginning of the wave path as displayed in Figure 18, we cannot use it as reference station since
501 there are no identified Love waves in the recordings. Both figures depict the very similar spatial
502 distribution of central frequencies and amplification coefficients during the two Chuetsu
503 earthquakes. In the areas of Tokyo and Chiba, the central frequency of prograde Rayleigh waves
504 is in the range 0.15-0.2 Hz, whereas for Love waves it is in the lower range 0.1-0.15 Hz. From
505 numerical simulations Kato et al. [16] had already identified Love waves of 0.125 Hz
506 propagating in Tokyo. It is important to point out that the coefficient of amplification for Love
507 waves is associated with higher values for this lower central frequency. Juxtaposed to the
508 response to the Tohoku event and being different from it, the spatial distribution of high
509 amplification of the prograde Rayleigh waves during the Chuetsu events is concentrated in the
510 Tokyo and Chiba areas, far from the edges. For Love waves we find *a very similar* spatial
511 distribution of the central frequencies during the Tohoku and two Chuetsu earthquakes (compare
512 Figures 13 and 20), suggesting that the central frequency of Love waves is strongly dependant on
513 the local geological structure. During the two Chuetsu events, we observe important

amplification on the stations next to the western edge, related to the generation of Love waves by that edge. Another similarity regarding Love waves induced in the basin by the three events is that the amplification coefficient in the southern Chiba area is not as strong as in the Tokyo and Saitama areas. The peak values of Love-wave amplification are observed in the vicinity of the Tokyo bay area. However, amplification during the Tohoku earthquake was three times larger than the amplification during the Chuetsu events, indicating that earthquake magnitude and azimuthal angle of the incident seismic energy may have a strong effect on the amplitude of Love waves.

Conclusions

We have identified and analyzed surface waves in the Nobi and Kanto basins in Japan, recorded during the Tohoku, Chuetsu and Chuetsu-oki earthquakes. We have extracted the waveforms of the different types of surface waves (retrograde Rayleigh, prograde Rayleigh and Love waves) and we have quantified their direction of polarization/propagation. We consider three earthquake events which allow us to perform comparisons among (a) a very large and two smaller events exciting the basins from different azimuths, and (b) two events ('twin' events) having close epicentral location and similar focal mechanisms. In order to quantify basin effects we measure the central frequency of the extracted waves and we estimate an amplification coefficient, giving for the first time a measure of amplification of extracted surface waves. We also present preliminary results of the relative group delay time t_{dr} of the basin generated surface waves (Love waves and prograde Rayleigh waves in the frequency range 0.1 – 0,5 Hz) in the Kanto basin during the 2011 Tohoku earthquake. We can summarize the findings of our study as follows:

- Low frequency (<0.1 Hz) seismic energy, in the form of retrograde Rayleigh waves arriving at Nobi during the Tohoku earthquake, does not interact with the basin. On the other hand, the higher frequency (0.1-0.5 Hz) Rayleigh waves incident on the basin, interact with the Nobi basin, being diffracted and amplified by it. The latter observation is in contrast to the fact that the (0.1-0.5 Hz) Rayleigh waves, arriving at Nobi during the two Chuetsu earthquakes, do not interact with the basin. We attribute this difference in response to the fact that for the Chuetsu events the azimuthal direction of incidence is very narrow as compared to that during the Tohoku earthquake. In the latter event, due to its great size, radiation is arriving at the Nobi basin over a considerably wider azimuthal range. Some of the azimuthal angles of the latter range may favor interaction of the basin with the incident Rayleigh waves in the frequency range 0.1-0.5 Hz.

- Seismic energy radiated by the Tohoku event, in the low frequency range (<0.1 Hz), consisting of retrograde Rayleigh waves was diffracted by the Kanto basin. One of the consequences of that diffraction was the generation of Love waves. The Kanto basin is deeper and considerably larger/wider as compared to the Nobi basin. This fact, along with the smooth velocity gradients with depth of the sediments, may have favored strong excitation of Love waves in the Kanto basin, as suggested also by Yoshimoto and Takemura [38], [57].

- Prograde Rayleigh waves and Love waves are observed in the Kanto basin (Tokyo lowlands and the Chiba area) in the frequency range 0.1-0.5 Hz. Conditions favoring the generation of prograde Rayleigh waves include the existence of very soft layers overlying very deep sediments. These conditions apparently exist in the Tokyo lowlands and the deeper parts of the Chiba sub-basin.

- It is important to note that Love waves (0.1-0.5 Hz) in the Kanto basin can reach as high as twice the amplitude of the Rayleigh waves in the same frequency range. This has important

implications for the torsional response of high-rise buildings and should be an important consideration in the design process of such important structures.

-The spatial distribution of the central frequency of the extracted Love waves was very similar for the three events, linking this central frequency to the local basin structure. Also, for all three events, the observed central frequencies of the Rayleigh waves were higher than those of the Love waves.

- For the three events, the peak values of Love wave amplification, were located in the vicinity of the Tokyo bay area, and are probably related to the saturation of the lowlands. However, amplification of Love waves during the Tohoku earthquake reached values three times higher than the peak values of amplification during the Chuetsu events. This indicates that amplification may be affected by the azimuthal direction of incidence.

- Both Chuetsu events (being 'twin' events as having the same magnitude and the same mechanism) generated very similar Rayleigh and Love waves, and very similar spatial distribution of amplification. This observation suggests that although the generation and propagation of seismic waves involve many uncertainties, key physical features of their generation and propagation are repeatable, and therefore can be modeled and predicted. It should be pointed out though that, as Mukai et al. [58] and Uetake [59] have demonstrated, factors such as the heterogeneous subsurface structure may affect, on occasion significantly, the seismic excitation and response of sedimentary basins. However, it is imperative that more events are analysed in order to identify patterns of generation/amplification of surface waves in sedimentary basins, so as to identify the factors that control their generation and intensity and, eventually, to develop the capability to predict them and synthesize them with confidence.

Data and Resources

All seismograms used in this work were recorded at K-NET stations, made available by the National Research Institute for Earth Science and Disaster Prevention (NIED) on their website (http://www.kyoshin.bosai.go.jp/, last accessed October 2019). The earthquake information was also provided by NIED (http://www.fnet.bosai.go.jp/, last accessed October 2019). The 3D models of bedrock depth for the Nobi and Kanto basins were retrieved from the 3D national deep structure model of NIED (http://www.j-shis.bosai.go.jp/, last accessed October 2019).

The relief geographic map of Japan in Figure 1 was generated with the code READHGT written by François Beauducel, from the Institute de Physique du Globe de Paris.

Acknowledgements

The authors are grateful for the comments of three anonymous reviewers that improved the clarity of the manuscript. This research has been financed by the French National Research Agency (Agence National de la Recherche), under project MODULATE, grant number ANR-18-CE22-0017.

References

[1] B. Gutenberg, "Effects of Ground on Earthquake Motion," *Bull. Seismol. Soc. Am.*, vol. 47, no. 3, pp. 221–250, 1957.

[2] K. Aki and K. L. Larner, "Surface Motion of a Layered Medium Having an Irregular Interface Due to Incident Plane SH Waves," *J. Geophys. Res.*, vol. 75, no. 5, pp. 933–954, 1970.

[3] P.-Y. Bard and M. Bouchon, "The Seismic Response of Sediment-Filled Valleys. Part 1. The Case of Incident SH Waves," *Bull. Seismol. Soc. Am.*, vol. 70, no. 4, pp. 1263–1286, 1980.

[4] P.-Y. Bard and M. Bouchon, “The Seismic Response of Sediment-Filled Valleys. Part 2. The Case of Incident P and SV Waves,” *Bull. Seismol. Soc. Am.*, vol. 70, no. 5, pp. 1921–1941, 1980.

[5] J. L. King and B. E. Tucker, “Observed Variations of Earthquake Motion across a Sediment-Filled Valley,” *Bull. Seismol. Soc. Am.*, vol. 74, no. 1, pp. 137–151, 1984.

[6] A. S. Papageorgiou and J. Kim, “Study of the propagation and amplification of seismic waves in Caracas Valley with reference to the 29 July 1967 earthquake: SH waves,” *Bull. Seismol. Soc. Am.*, vol. 81, no. 6, pp. 2214–2233, 1991.

[7] J. F. Hall and J. L. Beck, “Structural Damage in Mexico City,” *Geophys. J. Int.*, vol. 13, no. 6, pp. 589–592, 1986.

[8] R. W. Graves, “Modeling Three-Dimensional Site Response Effects in the Marina District Basin, San Francisco, California,” *Bull. Seismol. Soc. Am.*, vol. 83, no. 4, pp. 1042–1063, 1993.

[9] H. Kawase, “The cause of the damage belt in Kobe: ‘The basin-edge effect,’ constructive interference of the direct S-wave with the basin-induced diffracted/Rayleigh waves,” *Seismol. Res. Lett.*, vol. 67, no. 5, pp. 25–34, 1996.

[10] A. Frankel, W. Stephenson, and D. Carver, “Sedimentary basin effects in Seattle, Washington: Ground-motion observations and 3D simulations,” *Bull. Seismol. Soc. Am.*, vol. 99, no. 3, pp. 1579–1611, 2009.

[11] K. Koketsu, K. Hatayama, T. Furumura, Y. Ikegami, and S. Akiyama, “Damaging Long-period Ground Motions from the 2003 Mw 8.3 Tokachi-oki, Japan Earthquake,” *Seismol. Res. Lett.*, vol. 76, no. 1, pp. 67–73, 2005.

[12] K. Hatayama, T. Kanno, and K. Kudo, “Control factors of spatial variation of long-period strong ground motions in the Yufutsu sedimentary basin, Hokkaido, during the Mw 8.0 2003 Tokachi-oki, Japan, earthquake,” *Bull. Seismol. Soc. Am.*, vol. 97, no. 4, pp. 1308–1323, 2007.

[13] M. Çelebi, I. Okawa, T. Kashima, S. Koyama, and M. Iiba, “Response of a tall building far from the epicenter of the 11 March 2011 M9.0 Great East Japan earthquake and aftershocks,” *Struct. Des. Tall Spec. Build.*, vol. 24, no. July 2014, pp. 421–439, 2014.

[14] T. Furumura and T. Hayakawa, “Anomalous propagation of long-period ground motions recorded in Tokyo during the 23 October 2004 Mw 6.6 Niigata-ken Chuetsu, Japan, earthquake,” *Bull. Seismol. Soc. Am.*, vol. 97, no. 3, pp. 863–880, 2007.

[15] S. Kinoshita, H. Fujiwara, T. Mikoshiba, and T. Hoshino, “Secondary Love waves observed by a strong-motion array in the Tokyo lowlands, Japan,” *J. Phys. Earth*, vol. 40, no. 1, pp. 99–116, 1992.

[16] K. Kato, K. Aki, and T. L. Teng, “3-D simulations of surface wave propagation in the Kanto sedimentary basin, Japan - part 1: application of the surface wave Gaussian beam method,” *Bull. - Seismol. Soc. Am.*, vol. 83, no. 6, pp. 1676–1699, 1993.

[17] K. Hatayama, K. Matsunami, T. Iwata, and K. Irikura, “Basin-Induced Love Waves of the Osaka in the Eastern Basin,” *J. Phys. Earth*, vol. 43, pp. 131–155, 1995.

[18] K. Miyakoshi, M. Horike, and R. Nakamiya, “Long predominant period map and detection of resonant high-rise buildings in the Osaka Basin, western Japan,” *Bull. Seismol. Soc. Am.*, vol. 103, no. 1, pp. 247–257, 2013.

[19] K. Sato, K. Asano, and T. Iwata, “Long-period Ground Motion Characteristics of the

Osaka Sedimentary Basin during the 2011 Great Tohoku Earthquake," in *15 WCEE*, 2012, pp. 0–6.

[20] K. Asano *et al.*, "Modelling of wave propagation and attenuation in the Osaka sedimentary basin, western Japan, during the 2013 Awaji Island earthquake," *Geophys. J. Int.*, vol. 204, no. 3, pp. 1678–1694, 2016.

[21] K. B. Olsen, "Site Amplification in the Los Angeles Basin from Three-Dimensional Modeling of Ground Motion," *Bull. Seismol. Soc. Am.*, vol. 90, no. 6B, pp. S77–S94, 2000.

[22] M. A. Denolle, H. Miyake, S. Nakagawa, N. Hirata, and G. C. Beroza, "Long-period seismic amplification in the Kanto Basin from the ambient seismic field," *Geophys. Res. Lett.*, vol. 41, pp. 2319–2325, 2014.

[23] M. Horike, H. Uebayashi, and Y. Takeuchi, "Seismic Response in Three-Dimensional Sedimentary Basin due to Plane S Wave Incidence," *J. Phys. Earth*, vol. 38, no. 4, pp. 261–284, 1990.

[24] S. Takemura, M. Akatsu, K. Masuda, K. Kajikawa, and K. Yoshimoto, "Long-period ground motions in a laterally inhomogeneous large sedimentary basin : observations and model simulations of long-period surface waves in the northern Kanto Basin , Japan," *Earth, Planets Sp.*, vol. 67, no. 33, pp. 1–17, 2015.

[25] L. Viens, H. Miyake, and K. Koketsu, "Simulations of long-period ground motions from a large earthquake using finite rupture modeling and the ambient seismic field," *J. Geophys. Res. Solid Earth*, vol. 121, no. 12, pp. 8774–8791, 2016.

[26] L. Seydoux, N. M. Shapiro, J. De Rosny, and M. Landès, "Spatial coherence of the seismic

669 wavefield continuously recorded by the USArray," *Geophys. Res. Lett.*, vol. 43, pp. 9644–
670 9652, 2016.

671 [27] M. Wathelet, B. Guillier, P. Roux, C. Cornou, and M. Ohrnberger, "Rayleigh wave three-
672 component beamforming: signed ellipticity assessment from high-resolution frequency-
673 wavenumber processing of ambient vibration arrays," *Geophys. J. Int.*, vol. 215, no. 1, pp.
674 507–523, 2018.

675 [28] B. E. Tucker and J. L. King, "Dependence of sediment - filled valley response on input
676 amplitude and valley properties," *Bull. - Seismol. Soc. Am.*, vol. 74, no. 1, pp. 153–165,
677 1984.

678 [29] H.-L. Liu and T. Heaton, "Array analysis of the ground velocities and accelerations from
679 the 1971 San Fernando, California, earthquake," *Bull. Seismol. Soc. Am.*, vol. 74, no. 5, pp.
680 1951–1968, 1984.

681 [30] T. C. Hanks, "Strong Ground Motion of the San Fernando, California, Earthquake: Ground
682 Displacements," *Bull. Seismol. Soc. Am.*, vol. 65, no. 1, pp. 193–225, 1975.

683 [31] J. S. Barker, M. Campillo, F. J. Sánchez-Sesma, D. Jongmans, and S. K. Singh, "Analysis
684 of wave propagation in the Valley of Mexico from a dense array of seismometers," *Bull.*
685 *Seismol. Soc. Am.*, vol. 86, no. 6, pp. 1667–1680, 1996.

686 [32] E. Fukuyama and T. Mikumo, "Dynamic rupture propagation during the 1891 Nobi,
687 Central Japan, earthquake: A possible extension to the branched faults," *Bull. Seismol. Soc.*
688 *Am.*, vol. 96, no. 4 A, pp. 1257–1266, 2006.

689 [33] H. Sekiguchi and M. Yoshimi, "Broadband Ground Motion Reconstruction for the Kanto
690 Basin during the 1923 Kanto Earthquake," *Pure Appl. Geophys.*, vol. 168, no. 3–4, pp.

609–630, 2011.

[34] K. C. Meza-Fajardo, A. S. Papageorgiou, and J. F. Semblat, “Identification and extraction of surface waves from three-component seismograms based on the normalized inner product,” *Bull. Seismol. Soc. Am.*, vol. 105, no. 1, pp. 210–229, 2015.

[35] K. Ueshita and T. Sato, “Study on Subsidence of the Nōbi Plain,” in *10th International Conference on Soil Mechanics and Foundation Engineering (Stockholm). Environmental Control (incl Waste Materials).*, 1981.

[36] K. X.-S. Hao and H. Fujiwara, “Sedimentary Thickness In The Eastern Kanto Basin Estimated By All-Pass Receiver Function Using Dense Earthquake,” *14th World Conf. Earthq. Eng.*, pp. 10–15, 2008.

[37] NIED, “National Research Institute for Earth Science and Disaster Resilience, K-net, Kik-net,” 2019. .

[38] K. Yoshimoto and S. Takemura, “A study on the predominant period of long-period ground motions in the Kanto Basin , Japan,” *Earth, Planets Sp.*, vol. 66, no. 100, pp. 1–7, 2014.

[39] S. Kinoshita, “Kyoshin Net (K-NET),” *Seismol. Res. Lett.*, vol. 69, no. 4, pp. 309–332, 1998.

[40] R. G. Stockwell, L. Mansinha, and R. P. Lowe, “Localization of the Complex Spectrum: The S Transform,” *IEEE Trans. Signal Process.*, vol. 44, no. 4, pp. 998–1001, 1996.

[41] R. N. Bracewell, “The Fourier Transform and applications,” *McGraw Hill*, pp. 1–10, 2000.

[42] T. Furumura *et al.*, “Strong ground motions from the 2011 earthquake obtained from a dense nationwide seismic network,” *Recent Lanslides*, vol. 8, pp. 333–338, 2011.

[43] A. Frankel, “Rupture History of the 2011 M 9 Tohoku Japan Earthquake Determined from Strong-Motion and High-Rate GPS Recordings : Subevents Radiating Energy in Different Frequency Bands,” *Bull. Seismol. Soc. Americ*, vol. 103, no. 2, pp. 1290–1306, 2013.

[44] H. Kubo and Y. Kakehi, “Source process of the 2011 Tohoku earthquake estimated from the joint inversion of teleseismic body waves and geodetic data including seafloor observation data: Source model with enhanced reliability by using objectively determined inversion settings,” *Bull. Seismol. Soc. Am.*, vol. 103, no. 2B, pp. 1195–1220, 2013.

[45] K. C. Meza-Fajardo and A. S. Papageorgiou, “Estimation of rocking and torsion associated with surface waves extracted from recorded motions,” *Soil Dyn. Earthq. Eng.*, vol. 80, 2016.

[46] H. Miyake and K. Koketsu, “Long-period ground motions from a large offshore earthquake: The case of the 2004 off the Kii peninsula earthquake, Japan,” *Earth, Planets Sp.*, vol. 57, pp. 203–207, 2005.

[47] K. B. Olsen *et al.*, “TeraShake2: Spontaneous rupture simulations of Mw 7.7 earthquakes on the Southern San Andreas fault,” *Bull. Seismol. Soc. Am.*, vol. 98, no. 3, pp. 1162–1185, 2008.

[48] K. C. Meza-Fajardo and A. S. Papageorgiou, “Response of tall buildings to base rocking induced by Rayleigh waves,” no. January, pp. 1–19, 2018.

[49] P. Boué, M. Denolle, N. Hirata, S. Nakagawa, and G. C. Beroza, “Beyond basin resonance : Characterizing wave propagation using a dense array and the ambient seismic field,” *Geophys. J. Int.*, vol. 206, no. 2, pp. 1261–1272, 2016.

[50] T. Tanimoto and L. Rivera, “Prograde Rayleigh wave particle motion,” vol. 1, pp. 399–

405, 2005.

[51] K. Koketsu and M. Kikuchi, “Propagation of Seismic Ground Motion in the Kanto Basin , Japan,” vol. 288, no. May, pp. 1237–1240, 2000.

[52] Y. Cao, K. C. Meza-Fajardo, G. P. Mavroeidis, and A. S. Papageorgiou, “Effects of wave passage on torsional response of symmetric buildings subjected to near-fault pulse-like ground motions,” *Soil Dyn. Earthq. Eng.*, vol. 88, pp. 109–123, 2016.

[53] R. Gendrin *et al.*, “Wave packet propagation in an amplifying medium and its application to the dispersion characteristics and to the generation mechanisms of Pc 1 events,” *Planet. Space Sci.*, vol. 19, no. 2, pp. 165–194, 1971.

[54] M. B. Priestley, “Some Notes on the Physical Interpretation of Spectra of Non-Stationary Stochastic Processes,” *J. Sound Vib.*, vol. 17, no. 1, pp. 51–54, 1971.

[55] M. B. Priestley, “Evolutionary Spectra and Non-Stationary Processes,” *J. R. Stat. Soc. Ser. B*, vol. 27, no. 2, pp. 204–237, 1965.

[56] W. B. Joyner, “Strong motion from surface waves in deep sedimentary basins,” *Bull. Seismol. Soc. Am.*, vol. 90, no. 6 SUPPL., pp. 95–112, 2000.

[57] K. Yoshimoto and S. Takemura, “Surface wave excitation at the northern edge of the Kanto Basin, Japan,” *Earth, Planets Sp.*, vol. 66, no. 1, pp. 1–7, 2014.

[58] Y. Mukai, T. Furumura, and T. Maeda, “Causes of Azimuthally Dependent Amplification Variations of Long-period Ground Motions in the Kanto Basin, Central Japan,” *Bull. Earthq. Res. Inst.*, vol. 93, pp. 31–48, 2018.

[59] T. Uetake, “Effects of subsurface structures of source regions on long - period ground motions observed in the Tokyo Bay area , Japan,” *Earth, Planets Sp.*, 2017.

[60] R. Tajima and F. Tajima, “Seismic scaling relation of the 2007 Off Mid Niigata, Japan, earthquake (Mw 6.6) sequence in comparison with two other earthquake (Mw 6.6) sequences,” *Earth, Planets Sp.*, vol. 60, pp. 1137–1141, 2008.

Authors Affiliations

Kristel C. Meza-Fajardo

Risk and Prevention Division, BRGM.

3, avenue Claude-Guillemin, BP 36009 - 45060 Orléans cedex 2 – FRANCE

Tel: +33 (0) 2 38 64 36 91

E-mail: k.mezafajardo@brgm.fr

Hideo Aochi

Risk and Prevention Division, BRGM.

3, avenue Claude-Guillemin, BP 36009 - 45060 Orléans cedex 2 – FRANCE

E-mails: h.aochi@brgm.fr

Apostolos S. Papageorgiou

Department of Civil Engineering, University of Patras

GR-26500 Patras, Greece.

E-mail: papaga@upatras.gr

List of Figure Captions

Figure 1. The Nobi and Kanto basins. (a) Location of the basins (indicated by the squares), and locations of the epicenters of the events (indicated by stars), considered in this study. (b) Spatial distribution of K-NET stations in the Nobi basin. (c) Spatial distribution of K-NET stations in the Kanto basin. The contour plots indicate the depth corresponding to Vs=2700 m/s, with a level step of 500 m. For clarity, stations at Tokyo bay are not shown in (c). The stations codes at the Chiba sub-basin start with the letters CHB, at the Gunma-Saitama area with the letters GNM or SIT, and at the Tokyo bay area with letter TKY.

Figure 2. 3D deep structure model for a Vs=2700 m/s provided by NIED for (a) Kanto basin, and (b) Nobi basin. Whereas the Nobi basin apparently can be characterized as consisting of a single sub-basin, we can observe that the Kanto basin is composed of several sub-basins.

Figure 3. Displacement waveforms at rock stations during three different events. (a) Station SIT006 at Kanto basin, and (b) station GIF024 at Nobi basin. Zero pads have been added at the end of the recordings so that all time-histories have the same time length.

Figure 4. Amplitudes of the S-transform of vertical components recorded during three different events. (a) Station SIT006 at Kanto basin, and (b) station GIF024 at Nobi basin. We can observe the similarities in frequency content of the two Chuetsu events, with dominant frequencies between 0.1 and 0.2 Hz, at the two stations. For the Tohoku earthquake the dominant frequency at both stations evidently is below 0.1 Hz.

Figure 5. Extracted Rayleigh waves in the frequency range 0.05-0.1 Hz during the 2011 Tohoku earthquake propagating to the west in the Nobi basin. (a) Retrograde waves propagating to the West, (b) Retrograde waves propagating to the East. The direction of polarization in the horizontal component at each station is indicated on the top panels by the arrows. On the bottom

800 we display the time-histories of the horizontal and vertical components of extracted wave trains.
801 The time-history of the vertical component has been shifted 90 degrees with respect to the
802 horizontal component.
803 Figure 6. Extracted retrograde Rayleigh waves in the frequency range 0.05-0.1 Hz during the
804 2011 Tohoku earthquake propagating to the west in the Nobi basin. The direction of polarization
805 in the horizontal component at each station is indicated on the top panels by the arrows. On the
806 bottom we display the time-histories of the horizontal and vertical components of extracted wave
807 trains. The time-history of the vertical component has been shifted 90 degrees with respect to the
808 horizontal component.
809 Figure 7. Extracted Love waves in the range 0.05-0.1 Hz in Kanto basin during the 2011 Tohoku
810 earthquake in the Chiba area. The direction of polarization in the horizontal component at each
811 station is shown on the left panel. The right panel shows the time histories of the horizontal
812 component. In the case of Love waves, the direction of propagation is expected to be normal to
813 the direction of polarization.
814 Figure 8. Extracted Rayleigh waves in the frequency range 0.1-0.5 Hz during the 2011 Tohoku
815 earthquake. (a) Retrograde waves in the Kanto basin, (b) Prograde waves in the Kanto basin.
816 Figure 9. Extracted Retrograde Rayleigh waves in the frequency range 0.1-0.5 Hz during the
817 2011 Tohoku earthquake.
818 Figure 10. Particle motion of extracted Rayleigh waves in the R-Z plane during Tohoku
819 earthquake for 0.1-0.5 Hz. (a) Ellipse of retrograde Rayleigh wave at station SIT001 during 120-
820 140 s, (b) Ellipse of prograde Rayleigh wave at station CHB006 during 130-150 s. R (for ‘radial’)
821 denotes direction of maximum energy or direction of propagation, and Z denotes the vertical
822 direction.

823 Figure 11. Extracted Love waves in the range 0.1-0.5 Hz in Kanto basin during the 2011 Tohoku
824 earthquake. The direction of polarization in the horizontal component at each station is shown on
825 the left panel. The right panel shows the time histories of the horizontal component.
826 Figure 12. Amplification and central frequency of prograde waves in the range 0.1-0.5 Hz in
827 Kanto basin during the 2011 Tohoku earthquake. (a) Central frequency of extracted waves, (b)
828 Amplification coefficient $A1$.
829 Figure 13. Amplification and central frequency of Love waves in the range 0.1-0.5 Hz in Kanto
830 basin during the 2011 Tohoku earthquake. (a) Central frequency (Hz), (b) Amplification
831 coefficient $A1$.
832 Figure 14. Amplification of surface waves in the range 0.1-0.5 Hz in Kanto basin during the 2011
833 Tohoku earthquake. (a) Time delay for prograde Rayleigh waves (s), (b) Amplification
834 coefficient $A2$ for prograde Rayleigh waves, (c) Time delay for Love waves (s), (d)
835 Amplification coefficient $A2$ for Love waves.
836 Figure 15. Retrograde Rayleigh waves in the Nobi basin extracted in the frequency range 0.1-0.5
837 Hz. (a) During the Chuetsu earthquake, (b) during the Chuetsu-oki earthquake.
838 Figure 16. Retrograde Rayleigh waves in the Kanto basin extracted in the frequency range 0.1-0.5
839 Hz. (a) During the Chuetsu earthquake, (b) during the Chuetsu-oki earthquake.
840 Figure 17. Prograde Rayleigh waves in the Kanto basin extracted in the frequency range 0.1-0.5
841 Hz. (a) During the Chuetsu earthquake, (b) during the Chuetsu-oki earthquake.
842 Figure 18. Love waves in the Kanto basin extracted in the frequency range 0.1-0.5 Hz. (a) During
843 the Chuetsu earthquake, (b) during the Chuetsu-oki earthquake.
844 Figure 19. Amplification of prograde Rayleigh waves in the Kanto basin extracted in the
845 frequency range 0.1-0.5 Hz. (a) Central frequency (Hz) during the Chuetsu earthquake, (b)

Central frequency (Hz) during the Chuetsu-oki earthquake, (c) Amplification coefficient $A1$ during the Chuetsu earthquake, (d) Amplification coefficient $A1$ during the Chuetsu-oki earthquake.

Figure 20. Amplification of Love waves in the Kanto basin extracted in the frequency range 0.1-0.5 Hz. (a) Central frequency (Hz) during the Chuetsu earthquake, (b) Central frequency (Hz) during the Chuetsu-oki earthquake, (c) Amplification coefficient $A1$ during the Chuetsu earthquake, (d) Amplification coefficient $A1$ during the Chuetsu-oki earthquake.

854 **Tables and Figures**

Table 1. Earthquake events considered for surface wave analysis in Nobi and Kanto basins. Earthquake information is based on the catalogue of the Japan Meteorological Agency. Time is local time (JST).

Name	Event time	Magnitude M_{JMA}	Latitude	Longitude	Depth (Km)	Note
Niigata-Chuetsu[(1)]	2004/10/23 17:56:00	6.8	37.291	138.867	13	Crustal reverse faulting
Chuetsu-oki[(2)]	2007/07/16 10:13:22	6.8	31.557	136.608	17	Crustal reverse faulting
Tohoku[(3)]	2011/03/11 14:46:18	9.0	38.103	142.86	24	subduction

[(1)] [14]
[(2)] [60]
[(3)] [44]

855

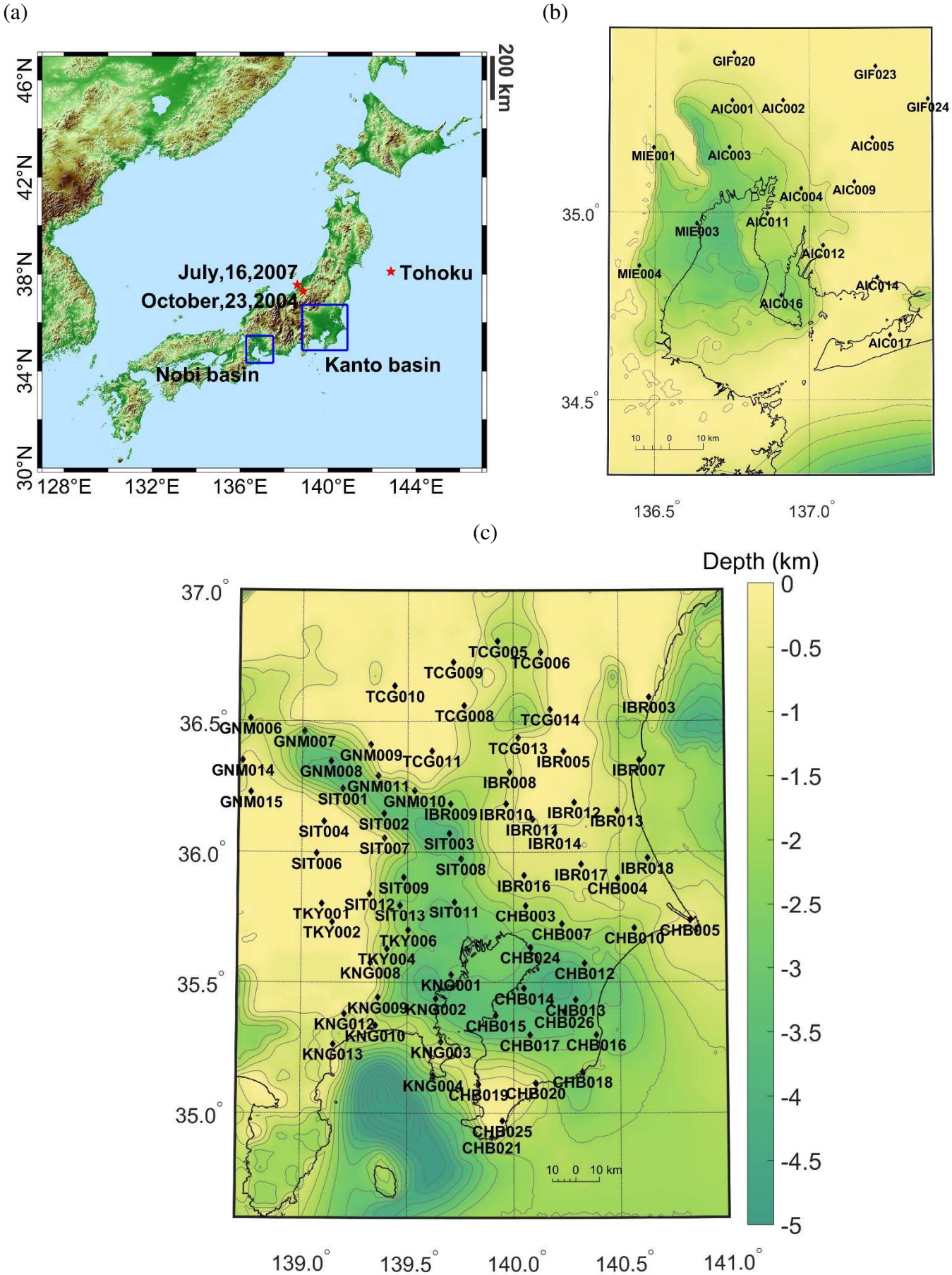

Figure 1. The Nobi and Kanto basins. (a) Location of the basins (indicated by the squares), and locations of the epicenters of the events (indicated by stars), considered in this study. (b) Spatial distribution of K-NET stations in the Nobi basin. (c) Spatial distribution of K-NET stations in the Kanto basin. The contour plots indicate the depth corresponding to Vs=2700 m/s, with a level step of 500 m. For clarity, stations at Tokyo bay are not shown in (c). The stations codes at the Chiba sub-basin start with the letters CHB, at the Gunma-Saitama area with the letters GNM or SIT, and at the Tokyo bay area with letter TKY.

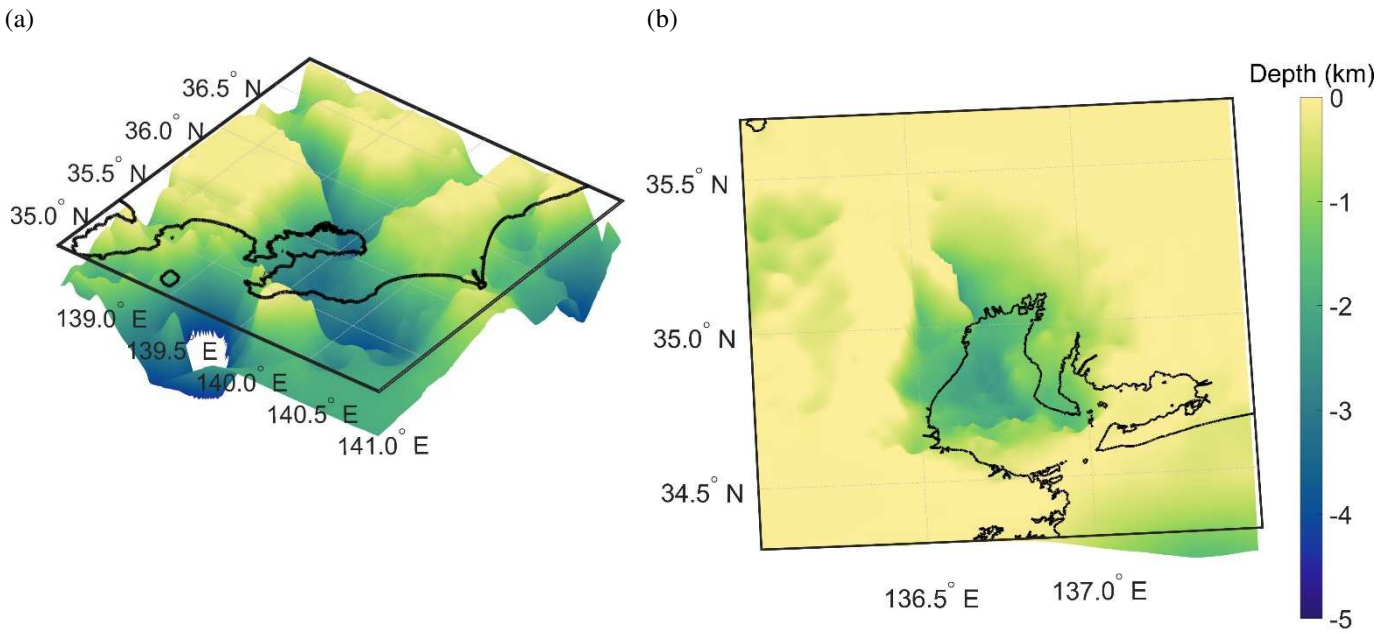

Figure 2. 3D deep structure model for a Vs=2700 m/s provided by NIED for (a) Kanto basin, and (b) Nobi basin. Whereas the Nobi basin apparently can be characterized as consisting of a single sub-basin, we can observe that the Kanto basin is composed of several sub-basins.

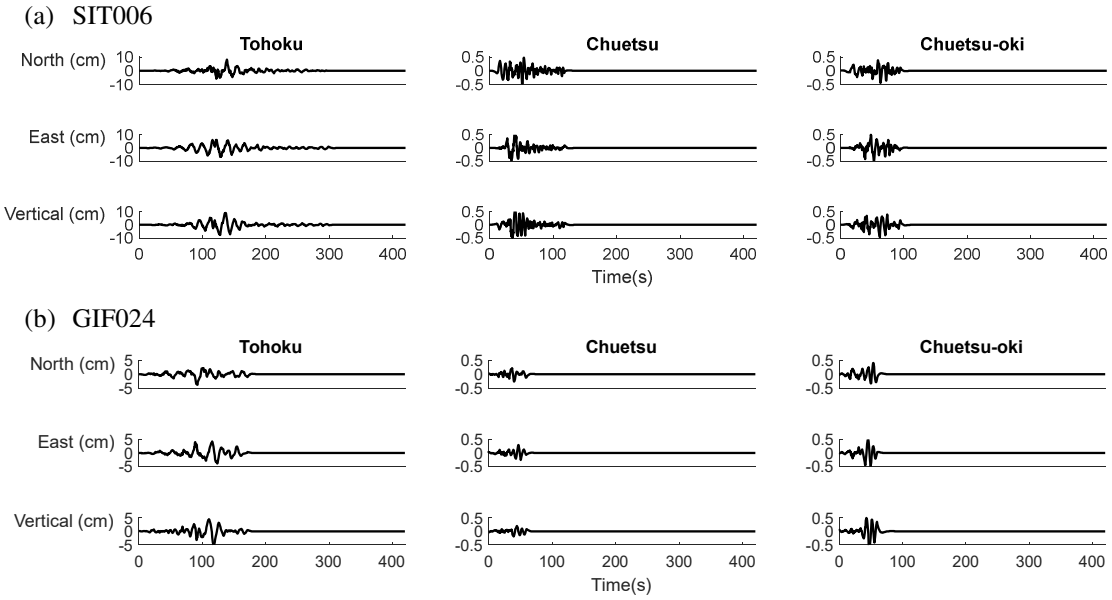

Figure 3. Displacement waveforms at rock stations during three different events. (a) Station SIT006 at Kanto basin, and (b) station GIF024 at Nobi basin. Zero pads have been added at the end of the recordings so that all time-histories have the same time length.

(a) SIT006

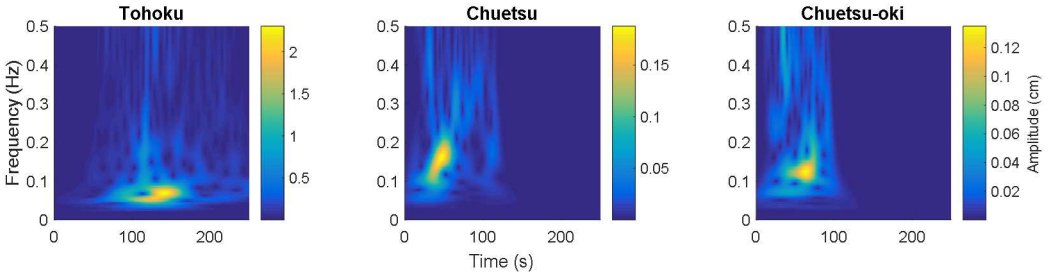

(b) GIF024

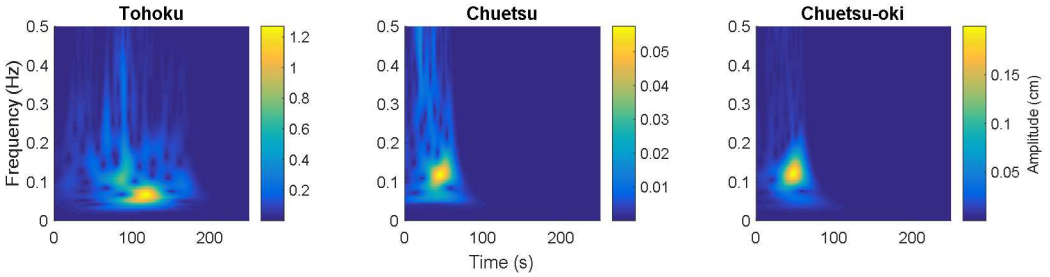

Figure 4. Amplitudes of the S-transform of vertical components recorded during three different events. (a) Station SIT006 at Kanto basin, and (b) station GIF024 at Nobi basin. We can observe the similarities in frequency content of the two Chuetsu events, with dominant frequencies between 0.1 and 0.2 Hz, at the two stations. For the Tohoku earthquake the dominant frequency at both stations evidently is below 0.1 Hz.

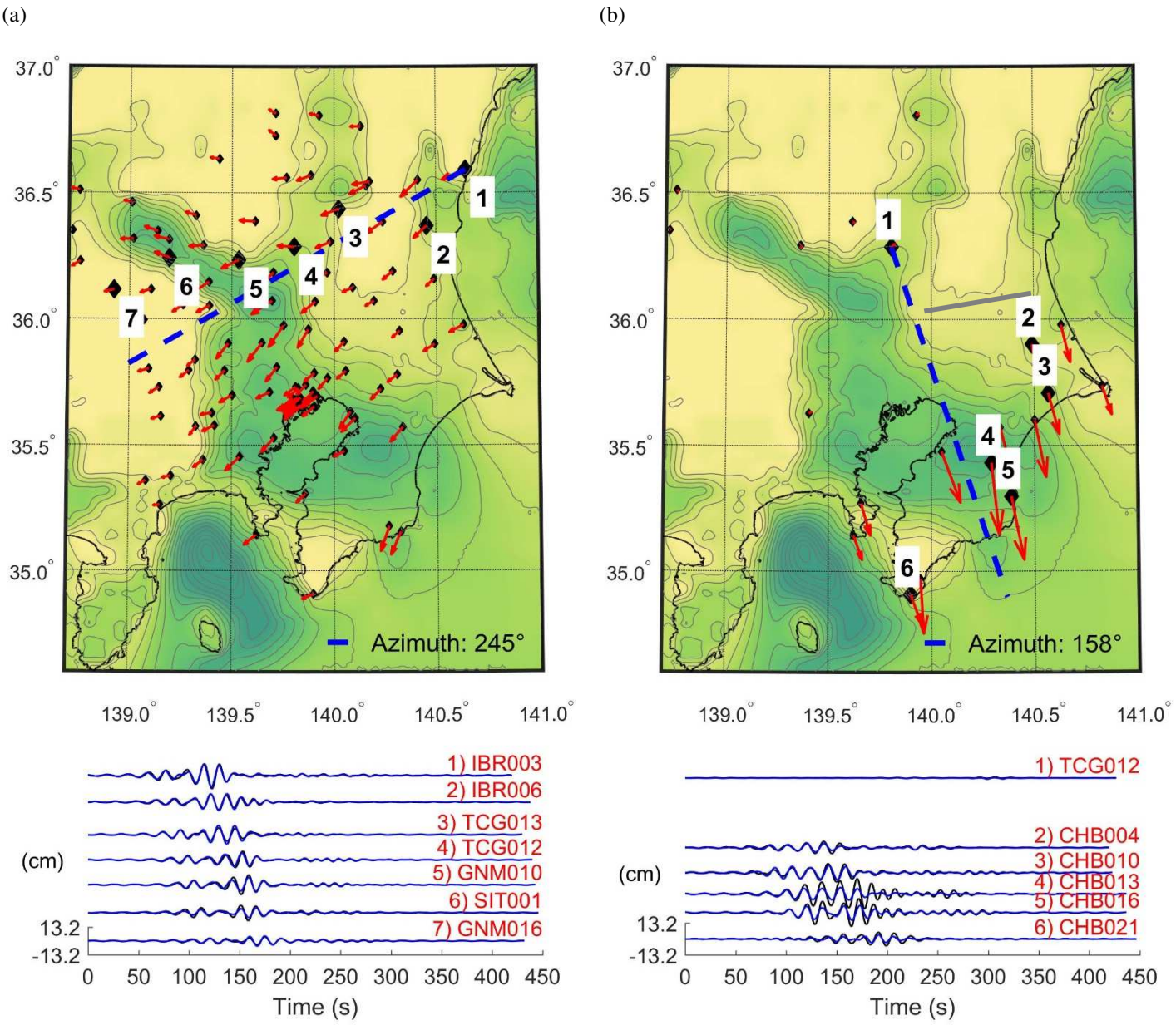

Figure 5. Extracted Rayleigh waves in the frequency range 0.05-0.1 Hz during the 2011 Tohoku earthquake propagating to the west in the Nobi basin. (a) Retrograde waves propagating to the West, (b) Retrograde waves propagating to the East. The direction of polarization in the horizontal component at each station is indicated on the top panels by the arrows. On the bottom we display the time-histories of the horizontal and vertical components of extracted wave trains. The time-history of the vertical component has been shifted 90 degrees with respect to the horizontal component.

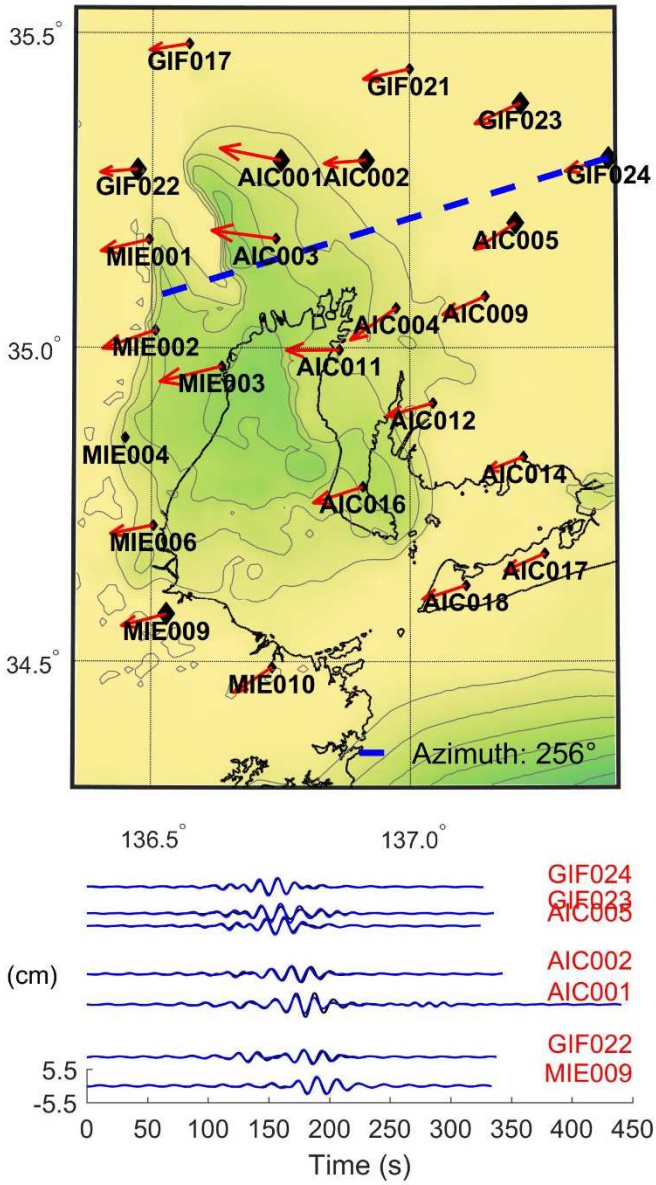

Figure 6. Extracted retrograde Rayleigh waves in the frequency range 0.05-0.1 Hz during the 2011 Tohoku earthquake propagating to the west in the Nobi basin. The direction of polarization in the horizontal component at each station is indicated on the top panels by the arrows. On the bottom we display the time-histories of the horizontal and vertical components of extracted wave trains. The time-history of the vertical component has been shifted 90 degrees with respect to the horizontal component.

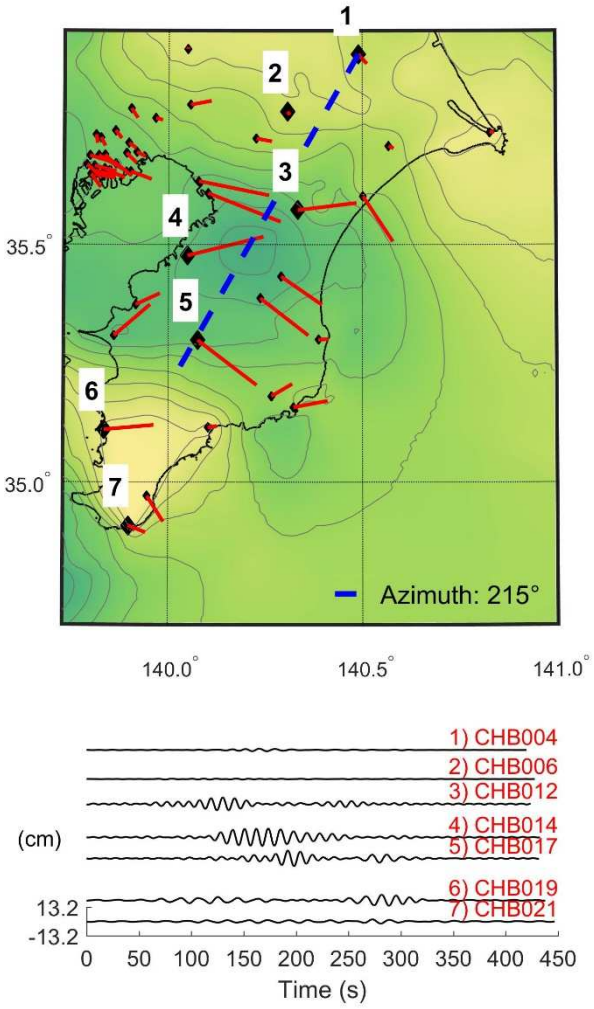

Figure 7. Extracted Love waves in the range 0.05-0.1 Hz in Kanto basin during the 2011 Tohoku earthquake in the Chiba area. The direction of polarization in the horizontal component at each station is shown on the left panel. The right panel shows the time histories of the horizontal component. In the case of Love waves, the direction of propagation is expected to be normal to the direction of polarization.

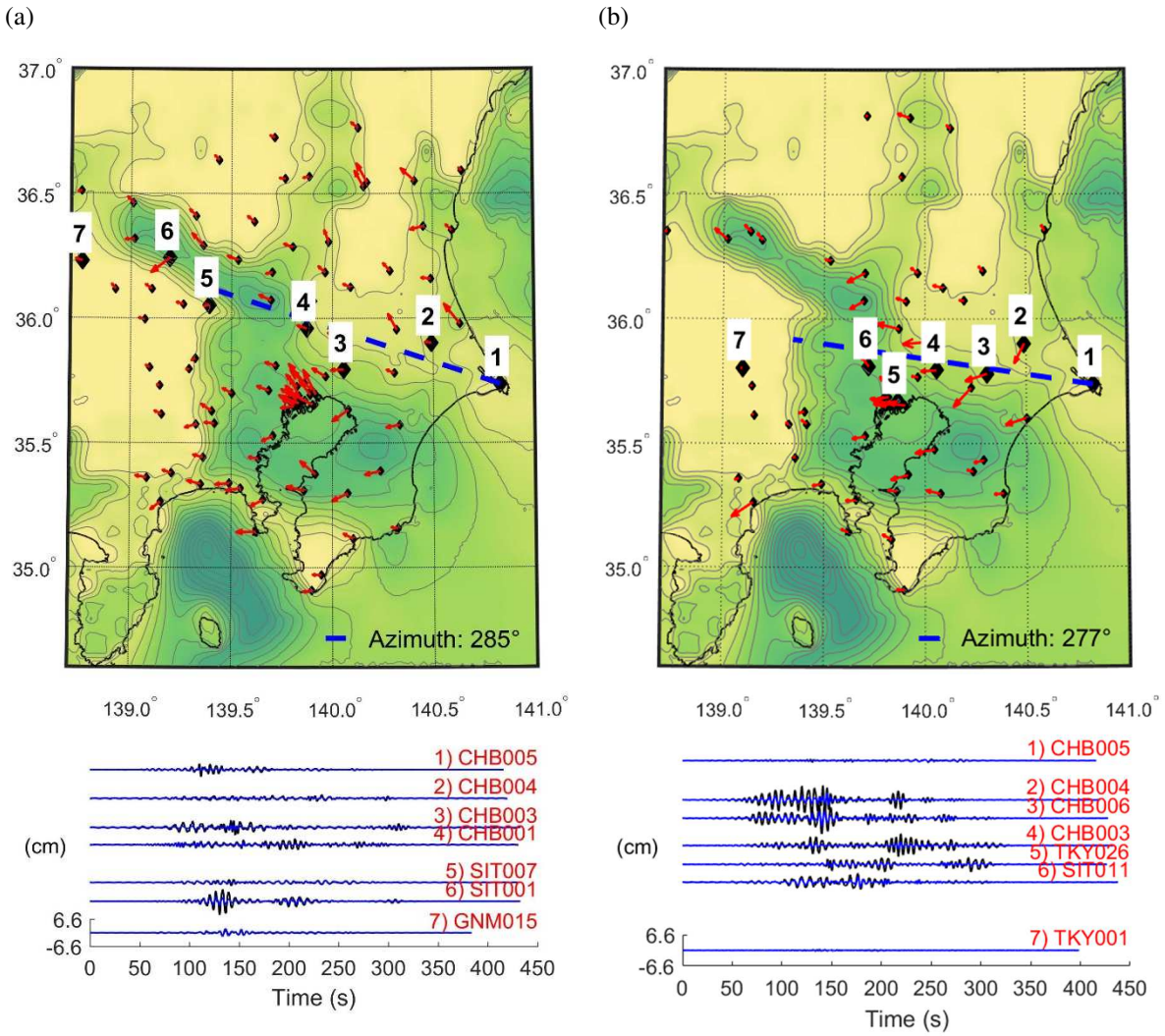

Figure 8. Extracted Rayleigh waves in the frequency range 0.1-0.5 Hz during the 2011 Tohoku earthquake. (a) Retrograde waves in the Kanto basin, (b) Prograde waves in the Kanto basin.

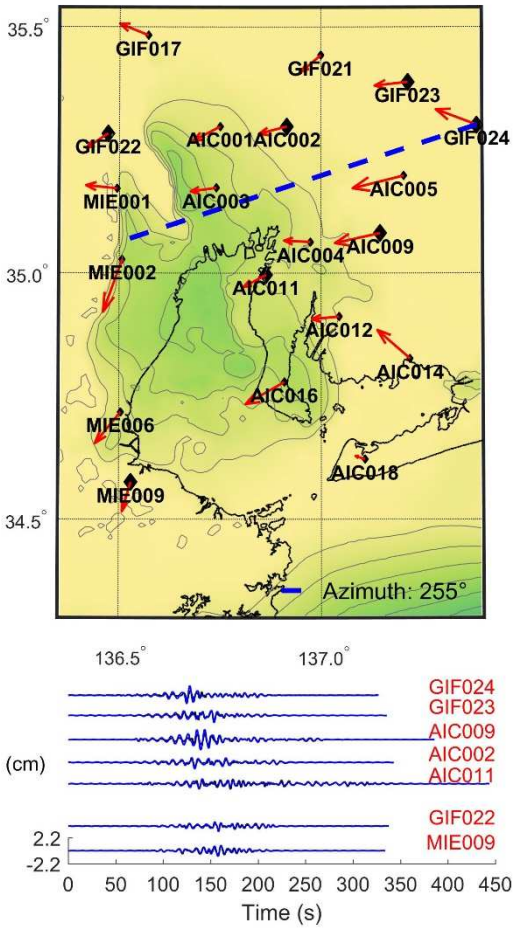

Figure 9. Extracted Retrograde Rayleigh waves in the frequency range 0.1-0.5 Hz during the 2011 Tohoku earthquake.

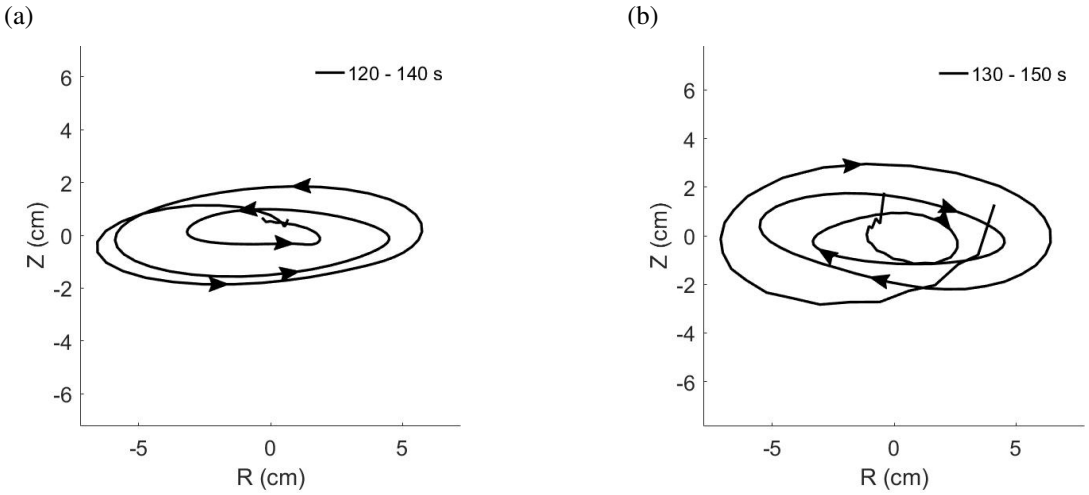

Figure 10. Particle motion of extracted Rayleigh waves in the R-Z plane during Tohoku earthquake for 0.1-0.5 Hz. (a) Ellipse of retrograde Rayleigh wave at station SIT001 during 120-140 s, (b) Ellipse of prograde Rayleigh wave at station CHB006 during 130-150 s. R (for 'radial') denotes direction of maximum energy or direction of propagation, and Z denotes the vertical direction.

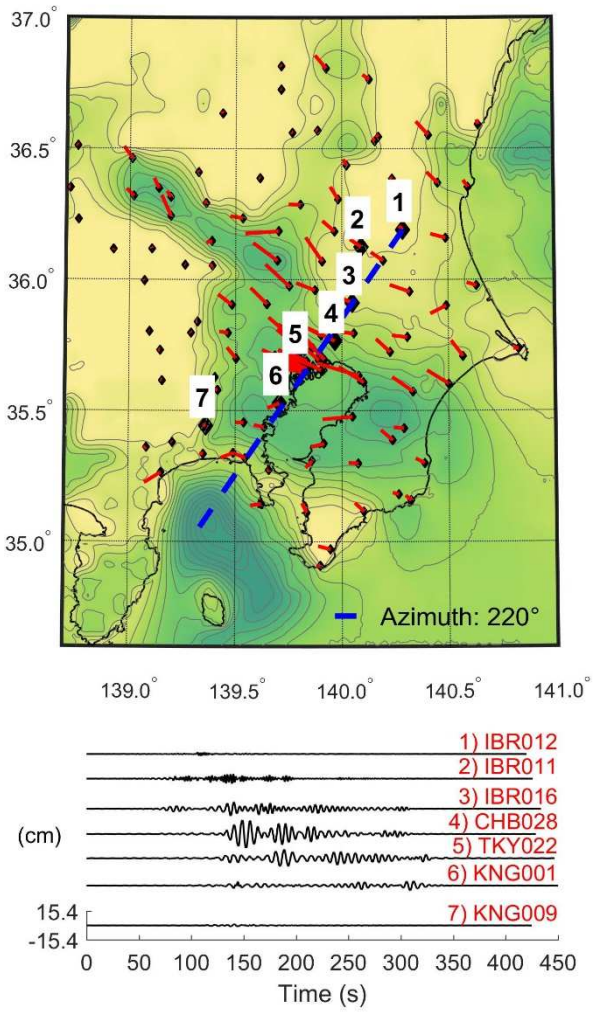

Figure 11. Extracted Love waves in the range 0.1-0.5 Hz in Kanto basin during the 2011 Tohoku earthquake. The direction of polarization in the horizontal component at each station is shown on the left panel. The right panel shows the time histories of the horizontal component.

(a) (b)

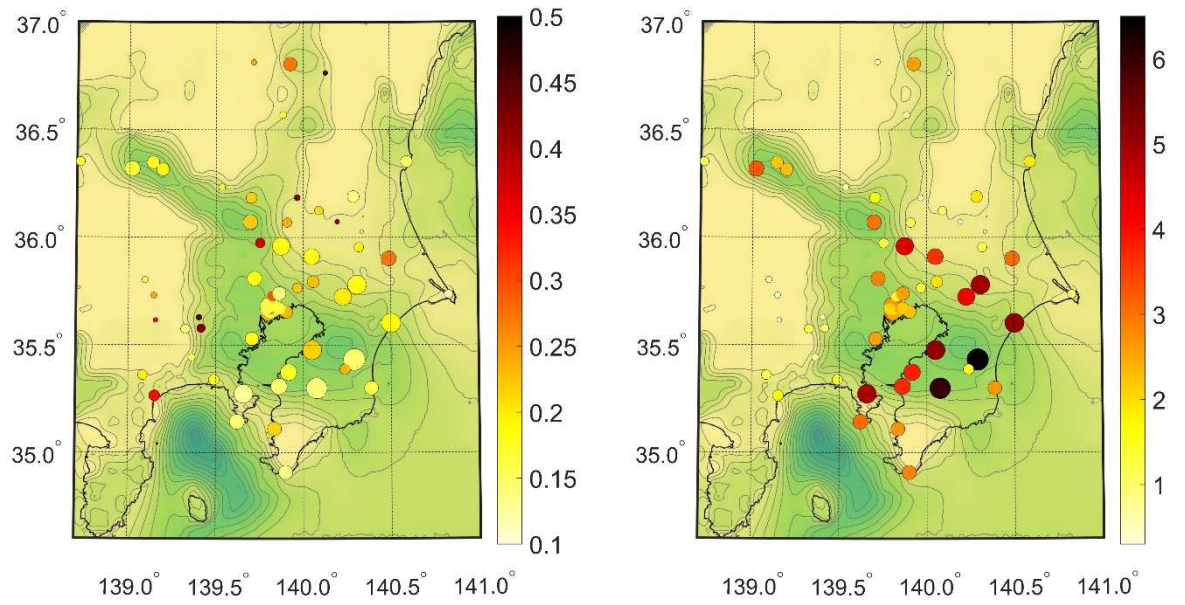

Figure 12. Amplification and central frequency of prograde waves in the range 0.1-0.5 Hz in Kanto basin during the 2011 Tohoku earthquake. (a) Central frequency of extracted waves, (b) Amplification coefficient A_1.

(a) (b)

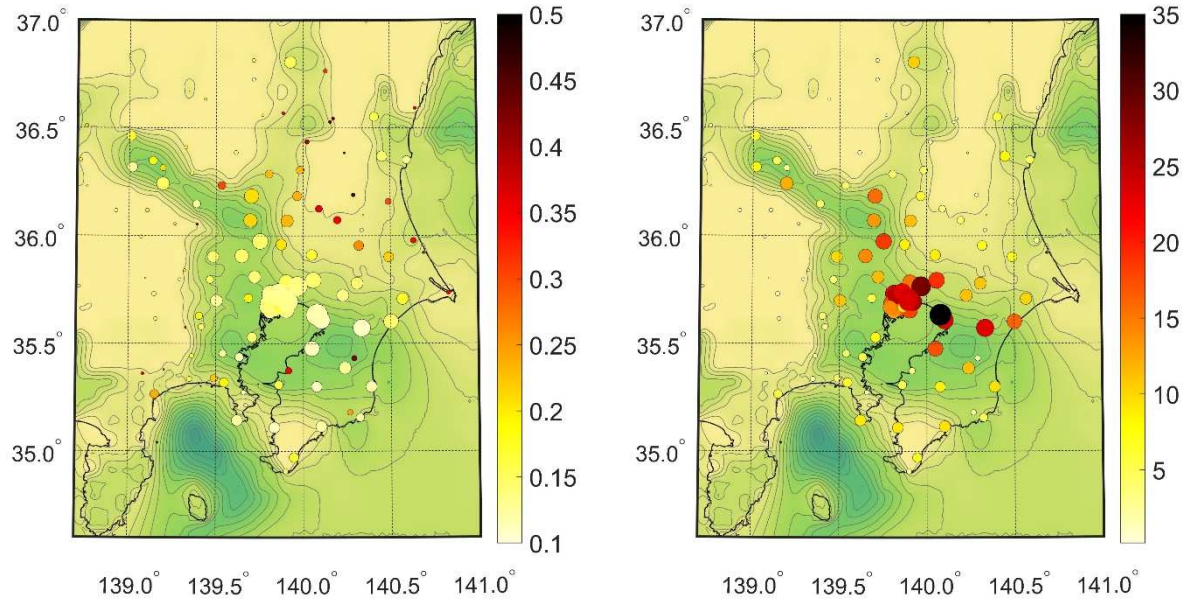

Figure 13. Amplification and central frequency of Love waves in the range 0.1-0.5 Hz in Kanto basin during the 2011 Tohoku earthquake. (a) Central frequency (Hz), (b) Amplification coefficient A_1.

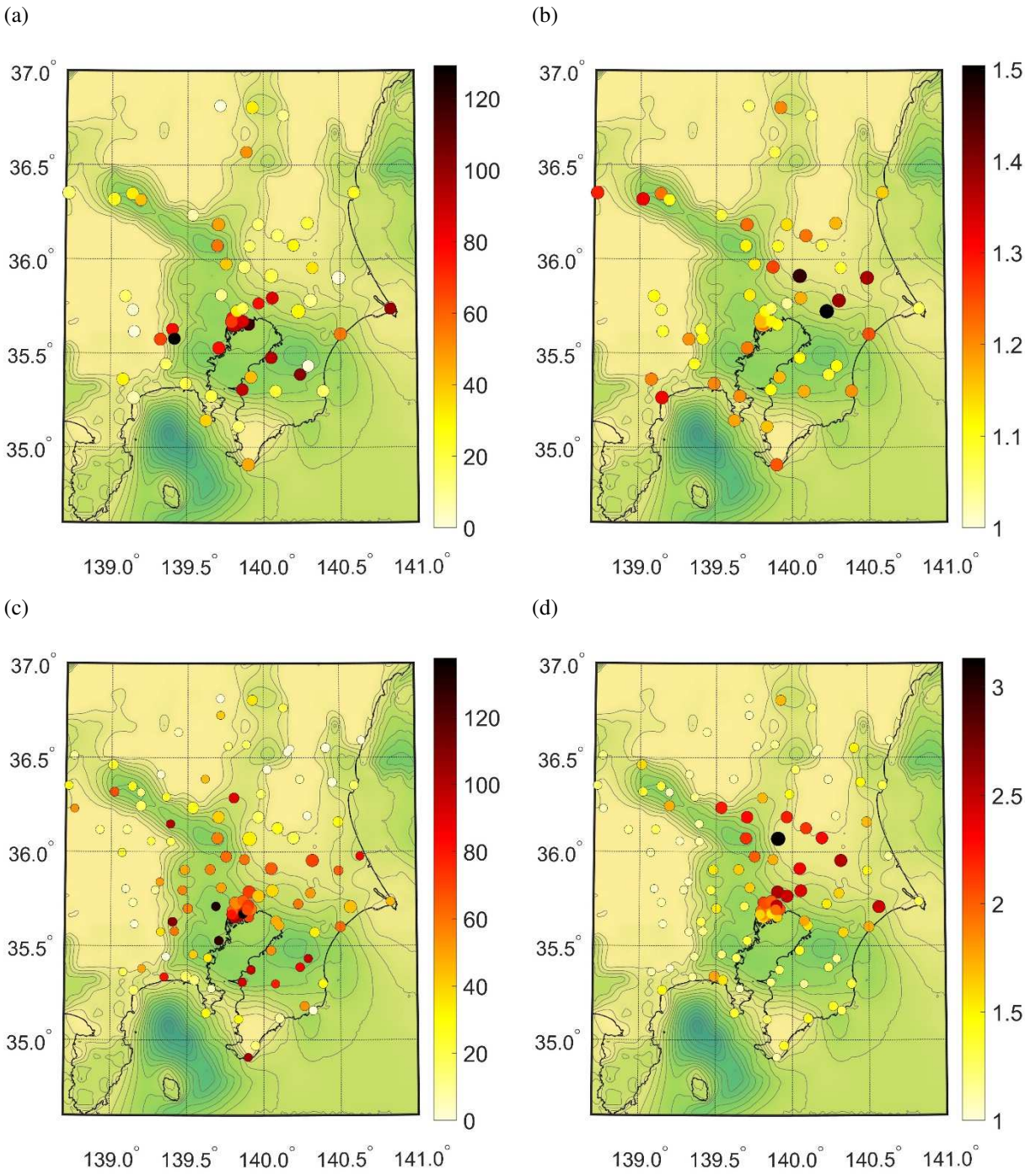

Figure 14. Amplification of surface waves in the range 0.1-0.5 Hz in Kanto basin during the 2011 Tohoku earthquake. (a) Time delay for prograde Rayleigh waves (s), (b) Amplification coefficient A_2 for prograde Rayleigh waves, (c) Time delay for Love waves (s), (d) Amplification coefficient A_2 for Love waves.

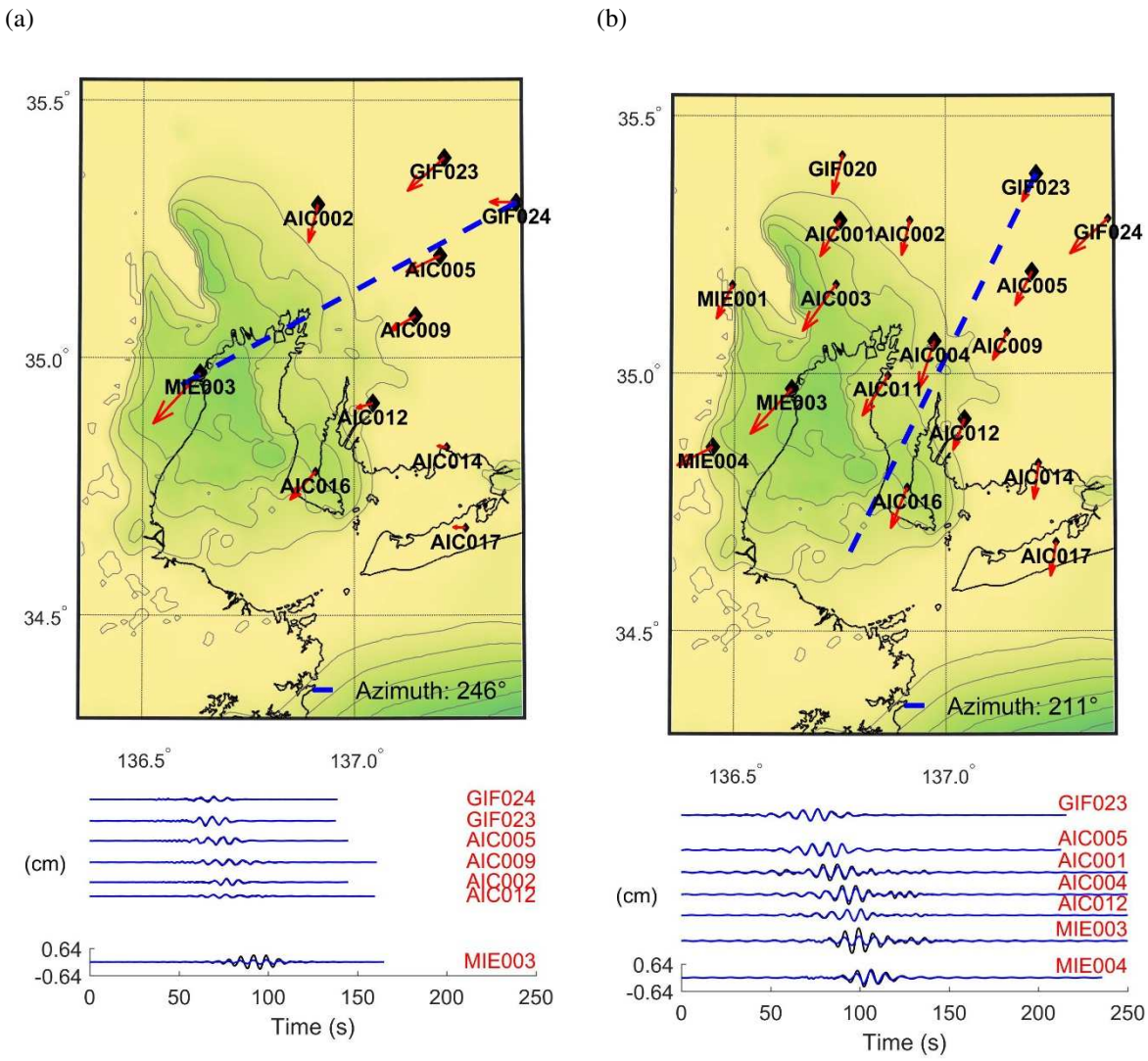

Figure 15. Retrograde Rayleigh waves in the Nobi basin extracted in the frequency range 0.1-0.5 Hz. (a) During the Chuetsu earthquake, (b) during the Chuetsu-oki earthquake.

(a) (b)

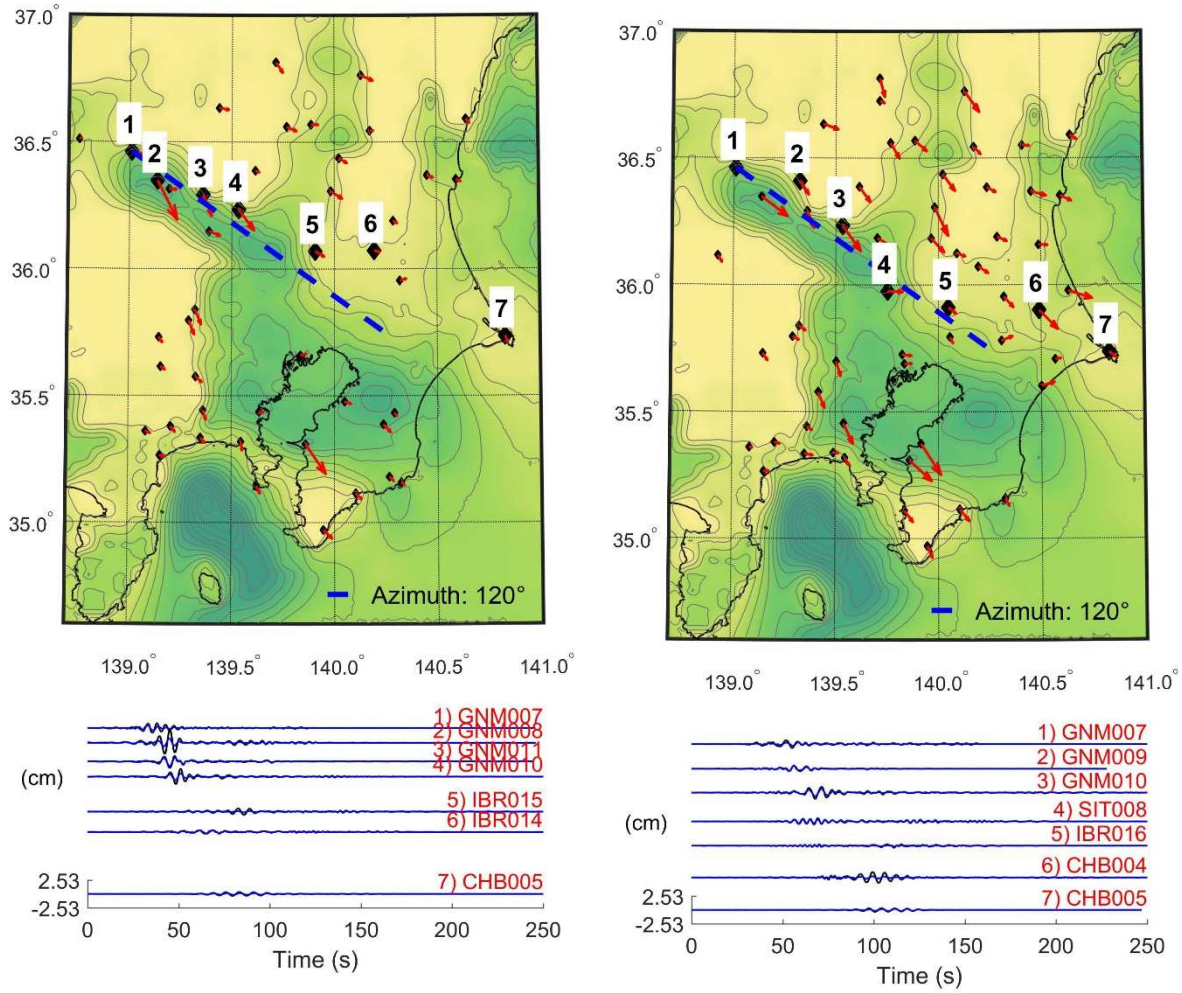

Figure 16. Retrograde Rayleigh waves in the Kanto basin extracted in the frequency range 0.1-0.5 Hz. (a) During the Chuetsu earthquake, (b) during the Chuetsu-oki earthquake.

(a) (b)

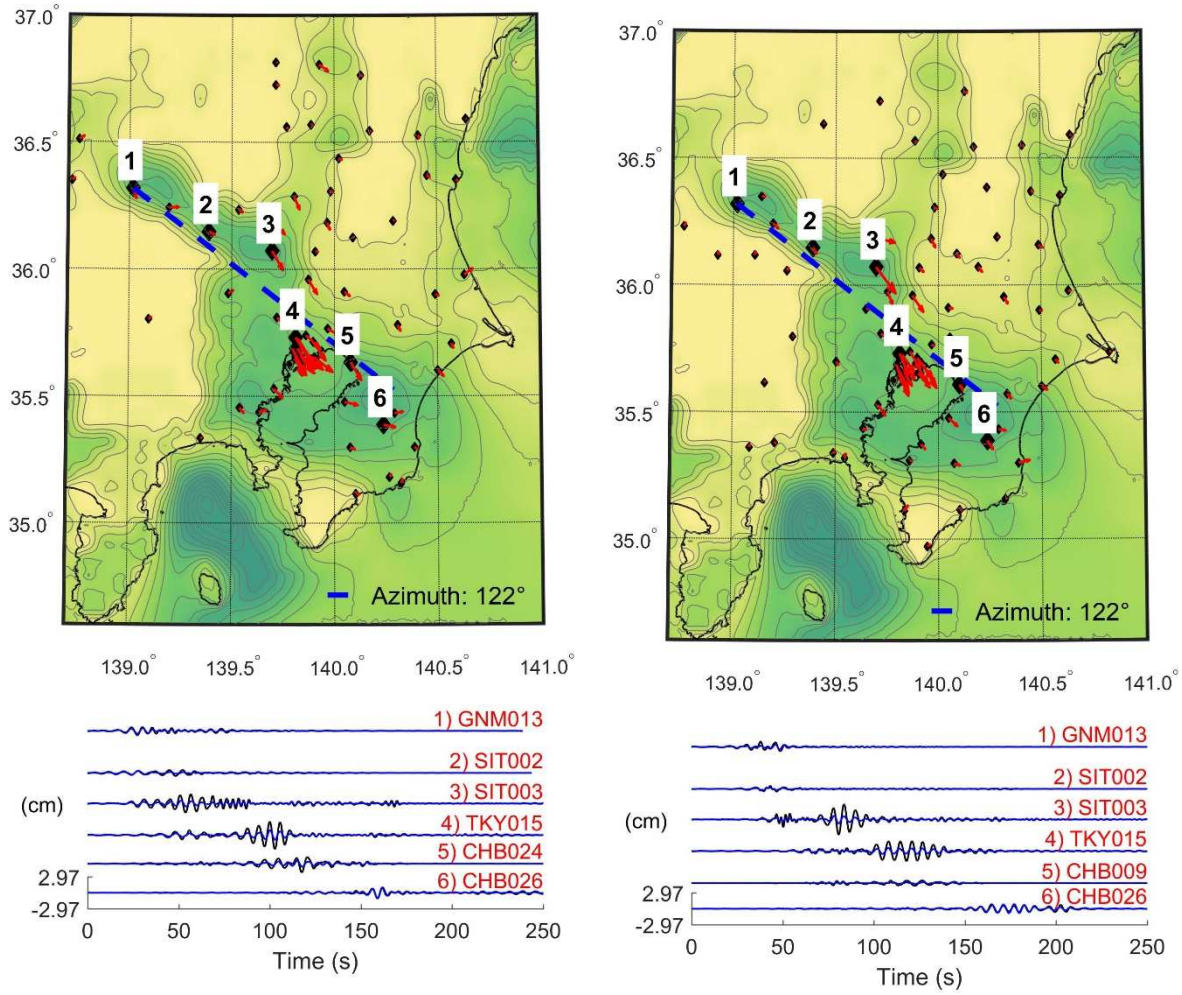

Figure 17. Prograde Rayleigh waves in the Kanto basin extracted in the frequency range 0.1-0.5 Hz. (a) During the Chuetsu earthquake, (b) during the Chuetsu-oki earthquake.

(a) (b)

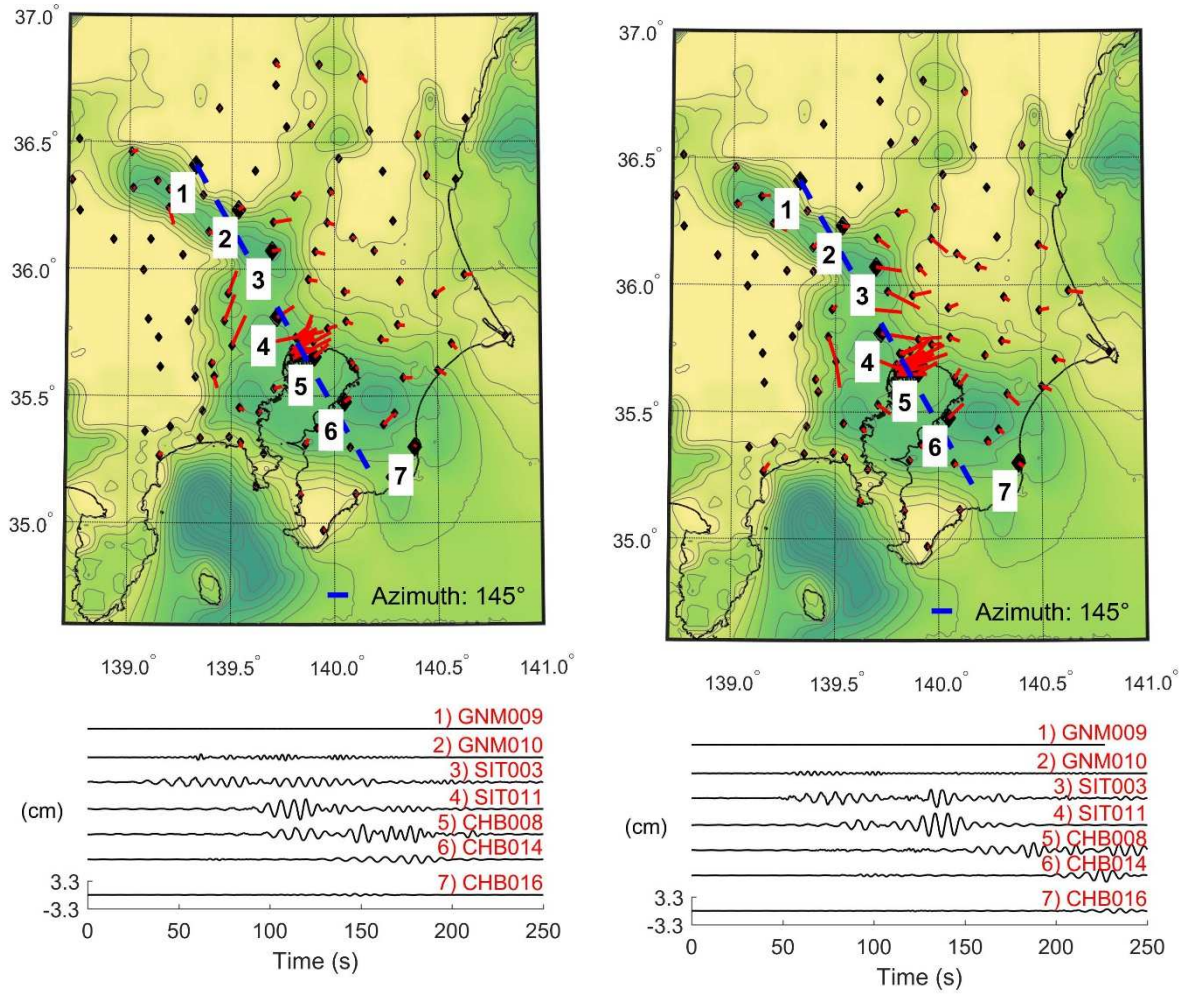

Figure 18. Love waves in the Kanto basin extracted in the frequency range 0.1-0.5 Hz. (a) During the Chuetsu earthquake, (b) during the Chuetsu-oki earthquake.

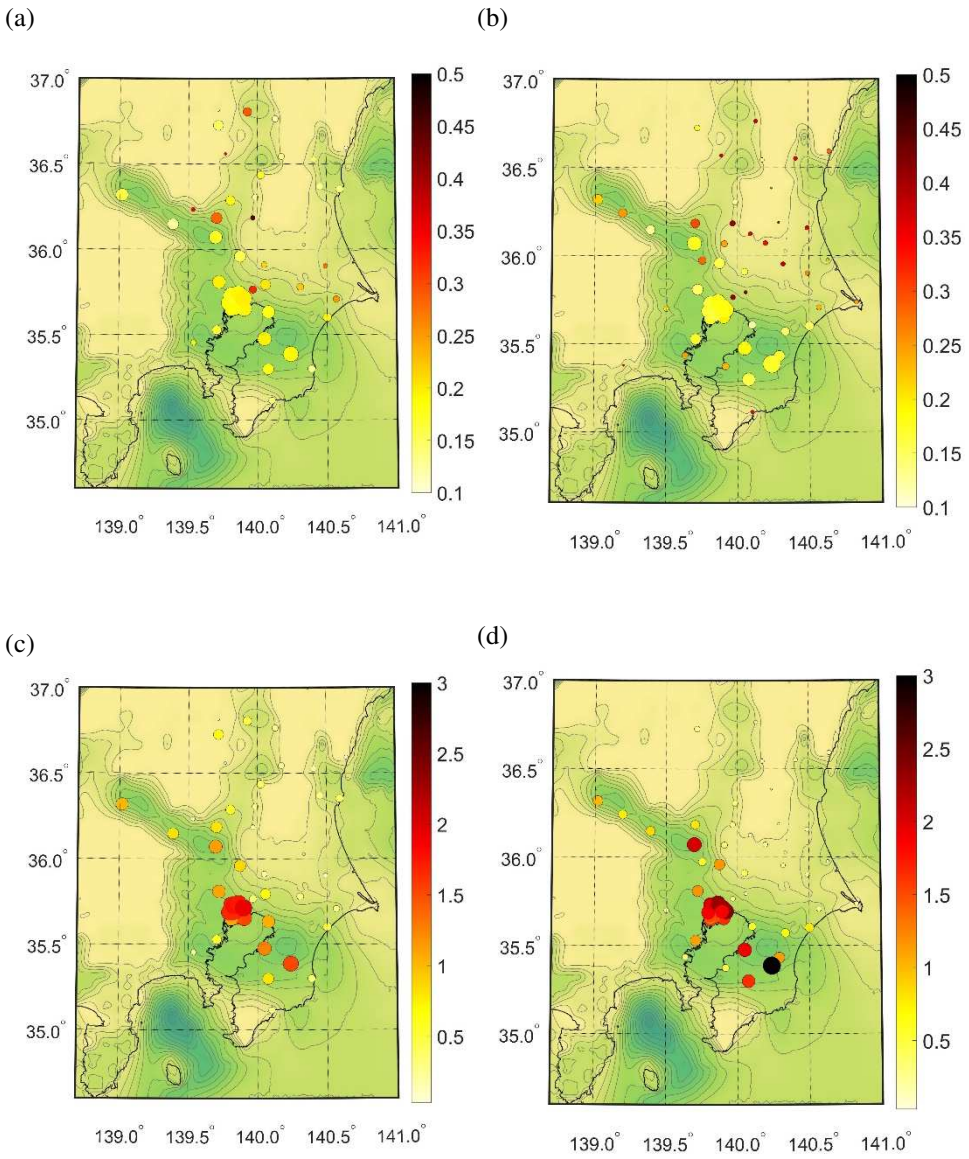

Figure 19. Amplification of prograde Rayleigh waves in the Kanto basin extracted in the frequency range 0.1-0.5 Hz. (a) Central frequency (Hz) during the Chuetsu earthquake, (b) Central frequency (Hz) during the Chuetsu-oki earthquake, (c) Amplification coefficient A_1 during the Chuetsu earthquake, (d) Amplification coefficient A_1 during the Chuetsu-oki earthquake.

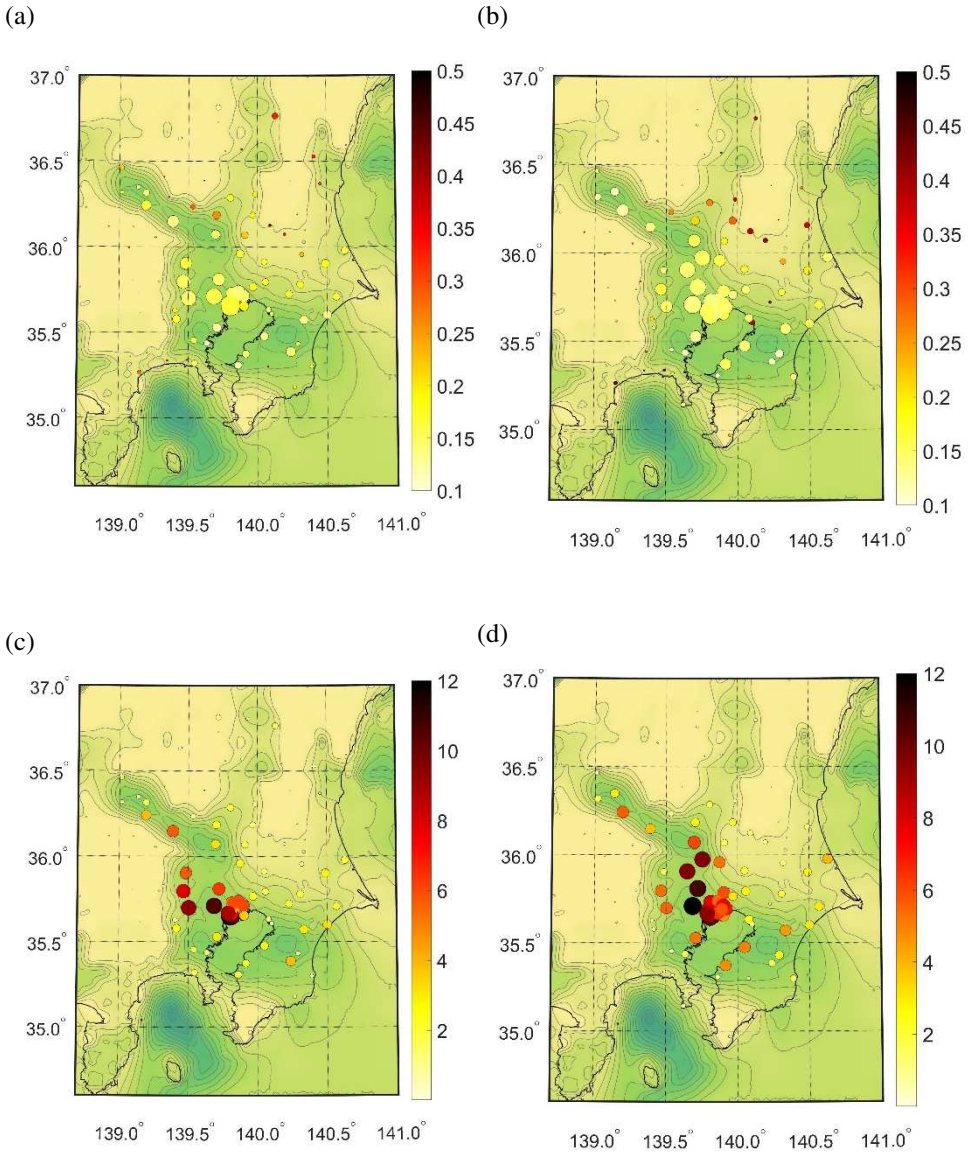

Figure 20. Amplification of Love waves in the Kanto basin extracted in the frequency range 0.1-0.5 Hz. (a) Central frequency (Hz) during the Chuetsu earthquake, (b) Central frequency (Hz) during the Chuetsu-oki earthquake, (c) Amplification coefficient A_1 during the Chuetsu earthquake, (d) Amplification coefficient A_1 during the Chuetsu-oki earthquake.